Forest Ecology and Management 595 (2025) 123002

Contents lists available at ScienceDirect

Forest Ecology and Management

journal homepage: www.elsevier.com/locate/foreco

# Comparison of digital aerial photogrammetry, lidar, and Sentinel-2 for evaluating forest fire effects

Bryce Frank [a,*], Jacob L. Strunk [a], Jeremy S. Fried [b], Karin Wolken [c], Sean C. McKenzie [d]

[a] USDA Forest Service, Pacific Northwest Research Station, 3625 93rd Avenue SW, Olympia, WA 98512, United States
[b] USDA Forest Service, Pacific Northwest Research Station, 1220 SW 3rd Avenue, Suite 1400, Portland, OR 97204, United States
[c] USDA Forest Service, Pacific Northwest Region, 1220 SW 3rd Avenue Ste. G015, Portland, OR 97204, United States
[d] Oregon Department of Forestry, Forest Resources Division – Forest Health Unit, 2600 State St, Salem, OR 97310, United States

ARTICLE INFO

*Keywords:*
Digital aerial photogrammetry
Lidar
Sentinel-2
Wildfires
Forest management
Fire effects

ABSTRACT

Wildfires have the potential to profoundly alter forest structure, which can leave land managers with severe information gaps when making post-fire forest management decisions. We assess point clouds derived from aerial lidar (16.8 points/m$^2$) and digital aerial photogrammetry (DAP, 13.9 points/m$^2$) for the purposes of generating post-fire forest attribute maps using 82 permanent field plots. Low-cost aerial lidar and DAP data can enable predictive mapping after fires occur, and an assessment of the utility of DAP in this context is warranted given its lower cost. We evaluated the performance of models constructed from post-fire lidar and DAP data collected over a 158,000 ha area formerly dominated by Douglas-fir in Oregon, United States for four forest attributes: live aboveground biomass, standing dead aboveground biomass, live stem density, and relative basal area change. Both data sources were augmented with Sentinel-2 pre- and post-fire images. DAP models had relative RMSEs that were 10–47 % larger than lidar models. Augmenting the models with Sentinel-2 narrowed this error differential to 3–16 %. We found that the difference between lidar and DAP heights is explained by lidar cover and canopy intensity, suggesting that consumption of canopy fuels can adversely affect the quality of DAP heights. Our results indicate that DAP models augmented with Sentinel-2 present an attractive prospect for fire footprints lacking lidar data owing to DAP's broader spatial and temporal availability; however, uncertainties may exist for some response variables in areas with high levels of canopy fuel consumption.

## 1. Introduction

Wildfires can render pre-fire forest inventory data obsolete in an instant, depriving forest managers of essential information they need to guide decisions about, for example, reforestation, hazard mitigation projects, salvage harvesting, and others (Larson et al., 2022; Lindenmayer et al., 2004; Rodman et al., 2024). In recent decades, remote sensing data from a variety of sources, such as multispectral satellite images, aerial lidar, and, more recently, point clouds constructed from digital aerial photogrammetry (DAP), have provided abundant low-cost auxiliary information. These data can, when paired with field observations, generate forest inventory and monitoring products potentially suited to mangers' post-fire inventory needs (Fassnacht et al., 2024; Tian et al., 2023).

Reliance on remote sensing data to assess the consequences of wildfires is a well-established operational practice. In the United States, a variety of data products, largely derived from multispectral satellite information, are routinely produced during and after wildfire events. These products address several objectives including emergency response planning, analysis of wildfire effects, forest management planning, and the development of public policy. The Monitoring Trends in Burn Severity (MTBS) program (Eidenshink et al., 2007; Picotte et al., 2020) publishes several data products for wildfires in the United States that are primarily derived from Landsat and Sentinel-2 images, including burned area boundaries, mapped predictions of burn severity classes, and estimates of areas within each burn severity class. Other programs that support wildfire assessments using remote sensing imagery include the Burned Area Emergency Response (BAER) program, which informs impact mitigation and recovery efforts post-fire (Clark et al., 2003), and Rapid Assessment of Vegetation Condition after Wildfire (RAVG)

* Corresponding author.
*E-mail address:* bryce.frank@usda.gov (B. Frank).

https://doi.org/10.1016/j.foreco.2025.123002
Received 28 March 2025; Received in revised form 8 July 2025; Accepted 11 July 2025
0378-1127/Published by Elsevier B.V.

program, which estimates and maps change in forest attributes like basal area and forest cover for large burn scars in federal forests managed by the United States Department of Agriculture (USDA) Forest Service (Baker et al., 2020). Both programs rely on multispectral images collected via satellite pre- and post-fire, enabling timely delivery of mapped fire effects products.

While multispectral imagery forms the foundation of these efforts, alternative remote sensing data sources that capture three-dimensional forest structure information provide increased predictive performance for many attributes of interest. Model performance is of special concern for forest managers, who are often tasked with planning forest inventory operations, including post-fire salvage harvesting, silvicultural treatments, and reforestation projects following fires, and require a level of predictive performance that multispectral images alone may not provide (Breidenbach et al., 2018; Temesgen et al., 2021). The increasingly common large-area (>10,000 ha) aerial lidar acquisitions in the western United States have been successfully harnessed to build predictive forest inventory models (Shin et al., 2016; Chamberlain et al., 2021; Winsemius et al., 2024). A growing literature reports the performance of lidar-driven forest inventory models in the context of wildfire effects, typically framed in the context of bi-temporal lidar acquisitions that capture pre- and post-fire attributes in an area of interest. For example, Hoe et al. (2018) found that pre-fire lidar-derived cover and lidar heights reduced root mean square errors in predicted change in live tree basal area in southwestern Oregon relative to a model based only on Landsat-derived relative differenced normalized burn ratio (RdNBR). Predictions of fuel consumption using bi-temporal lidar achieved $R^2$ values ranging between 0.40 and 0.67 (McCarley et al., 2020). Hu et al. (2019) developed a bi-temporal lidar data covariate, referred to as profile area change, that exhibited stronger correlations with change in basal area than changes in lidar height, lidar cover, or RdNBR. Forest managers look to lidar seeking timely (<= 2 years post-fire) characterization of the state of forest attributes such as live and dead biomass, yet most remote sensing studies of wildfire effects almost always focus on change prediction (e.g., Lentile et al., 2006). Some notable exceptions are Bohlin et al. (2017), which predicted proportions of fallen trees using bi-temporal lidar data, and Vogeler et al. (2016), which predicted post-fire wildlife habitat features, including presence of large dead trees. A more complete understanding is needed of what lidar can contribute to attributes of the post-fire environment that can support forest management decisions.

While lidar is the preeminent source of three-dimensional structural data used for forest inventory mapping in the Pacific Northwest, its application in modeling forest inventory post-fire can be complicated in practice. Aerial lidar acquisitions undertaken by public entities in the western United States are typically opportunistic and contingent on the availability of funding, interest, and operational capacity. As such, these lidar acquisitions form a spatiotemporal patchwork across the landscape (Mauro et al., 2021; Winsemius et al., 2024), and it is difficult to acquire pre- and post-fire lidar datasets with consistent technical specifications and extents. In contrast, DAP point clouds derived from aerial images can be produced in the western United States at regular two-year intervals for entire states due to the routine collection of aerial imagery by the National Agriculture Imagery Program (NAIP). These acquisitions ensure complete capture of post-fire landscapes within two years of all fires within a state, while obtaining three-dimensional structural information of the canopy surface (Mielcarek et al., 2020; Strunk et al., 2020).

While the spatial extent and temporal frequency of DAP acquisitions are a dramatic improvement in spatial breadth and temporal frequency over the existing "lidar patchwork", large-scale DAP acquisitions are still an emerging forest monitoring tool in the United States. As a result, many aspects of using DAP as a source of auxiliary information in forest inventory mapping are uncertain. This is especially the case for inventories following forest disturbance, where we uncovered only a handful of studies that investigate DAP in this context during literature review (Ali-Sisto and Packalen, 2016; Goodbody et al., 2018; Honkavaara et al., 2013), and were unable to find a comparable study that specifically investigates aerial DAP in the post-fire environment. Yet, there is reason to believe that the use of DAP for post-fire forest monitoring may involve additional challenges. For example, photogrammetric point clouds can exhibit artifacts such as omission or smoothing of lone trees, canopy edges, and gaps (Dietmaier et al., 2019; Strunk et al., 2019; Ritz et al., 2022), which may affect the reliability of point cloud data in a post-fire context where burned, branchless tree boles are abundant. This is especially germane for forest managers, who are often interested in this subpopulation of trees for the purposes of post-fire forest management. As a result, one of the most compelling contributions of this study is to demonstrate the potential for photogrammetric point clouds to support post-fire monitoring. This will enable forest managers to assess the strengths and weaknesses of DAP as a potential auxiliary data source.

This study was designed to directly compare lidar and DAP performances for post-fire forest monitoring. The first objective of this study was to evaluate the predictive performance of lidar and DAP for four management-relevant forest attributes: live aboveground biomass per hectare ($Mg \cdot ha^{-1}$), standing dead aboveground biomass per hectare ($Mg \cdot ha^{-1}$), live stem density ($trees \cdot ha^{-1}$), and relative basal area change. The second objective was to compare the relative contributions of different predictor types from lidar and DAP for each of the investigated attributes. Our third objective was to seek an understanding of discrepancies between the properties of lidar and DAP canopy heights, and to understand why these data products sometimes disagree. Our study is conducted over two of six high severity, wind-driven wildfires that burned over 300,000 ha of forest on the western slopes of the Cascade Mountains in western Oregon and southwest Washington, United States, on and immediately after Labor Day, 2020 (Busby et al., 2023).

## 2. Materials

### 2.1. Study region

In September of 2020, six synchronous high severity wildfires burned across the Cascades region of Oregon and Washington, United States, referred to as the Labor Day fires. The Beachie Creek and Lionshead fires were the two largest, composing nearly half of the total burned area, or approximately 158,000 ha. Our study region covered the majority of the Beachie Creek and Lionshead fires and is defined as the intersection of the fire boundaries and the footprint of a post-fire aerial lidar acquisition (Fig. 1). Most of the area burned by the Beachie Creek and Lionshead fires is located on the western side of the Cascade mountain range in Oregon, which has a warm-summer Mediterranean climate classification under the Köppen climate classification (Beck et al., 2023). The study region encompasses a dramatic east-west elevation gradient (185 m to 3048 m), which drives decreasing temperatures and increasing precipitation as elevation increases. Prior to the fires, this area was heavily forested with temperate forest species common in the Pacific Northwest region of the United States, including *Pseudotsuga menziesii* (Mirb.) Franco, *Tsuga heterophylla* (Raf.) Sarg., and *Tsuga mertensiana* (Bong.) Carr. Canopy cover was nearly continuous owing to high forest productivity and low fire frequency. The fires in this study region burned at high severity, involving large areas of stand replacing crown fires. Structurally, the resulting post-fire forest conditions were largely composed of burnt trees with little remaining canopy structure, but prevalent lower severity and unburned areas also existed at the lower and higher elevation areas within the burn perimeter (Fig. 1). These fires burned through forests in a heterogenous matrix of ownership classes, including federally owned forests, wilderness areas, state lands managed by the Oregon Department of Forestry, and private timberlands. The fire boundaries used in this study to define the post-fire area of interest are obtained from the Monitoring Trends in Burn Severity (MTBS) program (Eidenshink et al., 2007; Picotte et al., 2020).


**Fig. 1.** A map of the study region including portions of the Beachie Creek (west) and Lionshead (east) fires situated in the state of Oregon, United States. The approximate locations of forest inventory plots (actual locations are confidential) included in the analysis are indicated by white circles. A post-fire Sentinel-2 image is displayed in the background.

### 2.2. Field data

Field data were obtained from the national forest inventory of the United States administered by the USDA Forest Service Forest Inventory and Analysis (FIA) program. In this region of the United States, the FIA program uses a set of permanent plots that are revisited periodically over time such that each plot is measured approximately once every ten years. In Oregon, the FIA program uses varying sampling intensities, with a rectangular systematic grid used in some federally owned forests and a less dense quasi-systematic sampling design for other lands (Reams et al., 2005). The sample in this study is composed of plots from both sampling intensities. Plots from federally owned forests are primarily concentrated in the east of the study region and plots on non-federal forests are primarily in the west. The field plots in this national forest inventory are composed, in part, of four 7.3 m radius subplots, on which trees larger than 12.7 cm diameter at breast height are measured on a total plot area of approximately 670 $m^2$. The national forest inventory plots measured in this region contain other components, such as microplots used to measure small trees and downed woody material transects (Bechtold and Scott, 2005), however, we only used trees measured on the 7.3 m subplots for this study. The post-fire plot measurements we used in this study were collected for the Fire Effects and Recovery Study (FERS), which has collected remeasurement data on FIA plots within fire perimeters, typically within one year of the fire event, when funding and logistical flexibility permit. For the purposes of model development, we discarded any nonsampled plot, which occurred when any portion of the plot was deemed inaccessible by field crews, e.g., due to the presence of hazardous conditions. We also removed three plots that experienced timber harvesting between the field measurement date and the lidar acquisition date. After removing nonsampled plots and harvested plots, a total sample size of 82 field plots was available for model development.

We calculated four attributes of interest relevant for post-fire forest management on each field plot. Two of the attributes quantify the live and standing dead biomass pools, respectively. First, biomass predictions for each live and dead tree were obtained from the National Scale Volume and Biomass (NSVB) system of allometric models (Westfall et al., 2024). For the specific case of standing dead trees, aboveground biomass is modified by applying reductions to wood density, bark biomass, and branch biomass based on a decay class code determination made by field crews (USDA Forest Service, 2023; Westfall et al., 2024). To calculate a plot-level value for each of these biomass pools, the sum of tree-level biomasses within the pools is taken and then divided by the plot area of approximately 0.067 ha. Relative basal area change is obtained using the most recent pre-fire measurements of the same set of field plots to obtain pre-fire live basal area. Basal area that transferred from the live to dead pools due to fire was calculated from pre- and post-fire tree measurements. The quotient of the fire-killed basal area pool and the pre-fire live basal area pool was taken and forms the relative basal area change, with values of one indicating complete transfer of pre-fire live basal area in trees exceeding 12.7 cm to the pool of fire-killed basal area. Given that this attribute is a ratio, the denominator must be greater than zero, but some plots had no pre-fire live trees exceeding 12.7 cm, typically in recently harvested areas. This resulted in the elimination of an additional 18 plots, leaving 64 for analysis of this attribute. Live aboveground biomass and standing dead aboveground biomass are important for identifying potential timber value. Relative basal area change, a measure of change between pre- and post-fire forest structure, is a commonly used measure of fire severity in the region (e.g., Hoe et al., 2018). Similar quantities are produced in other products derived from multispectral data, including maps produced by the RAVG program (Miller et al., 2009). Finally, live stem density can be used in downstream data products as a proxy for seed tree availability, stocking, presence or absence of live trees, and to identify prospective tree-planting locations. Live stem density is calculated by dividing the number of live trees on the plot by the plot area. The attributes are summarized in Table 1. We highlight here that live aboveground biomass and live stem density both exhibit extreme right skew, which can be seen in the small differences between the medians and 25th percentiles. Indeed, many plots contain zero values for both attributes, owing to the severity of the fire within the study region (Fig. 1).

**Table 1**
Description of post-fire forest attributes used to form response variables. All attributes are calculated for trees greater than or equal to 12.7 cm diameter at breast height.

| Attribute | Median (25th, 75th percentile) | n |
|---|---|---|
| Live aboveground biomass ($Mg \cdot ha^{-1}$) | 4.0 (0.0, 179.0) | 82 |
| Standing dead aboveground biomass ($Mg \cdot ha^{-1}$) | 59.6 (5.4, 177.9) | 82 |
| Live stem density ($Trees \cdot ha^{-1}$) | 14.9 (0.0, 189.6) | 82 |
| Relative basal area change (Unitless) | 0.57 (0.11, 1.00) | 64 |

## 2.3. Remote sensing data

### 2.3.1. Lidar point clouds

The Oregon Department of Forestry commissioned a post-fire lidar acquisition for the study area in the summer of 2022 during leaf-on conditions. The acquisition was provided by GeoTerra, Inc., and used an Optech Galaxy T2000 lidar sensor mounted on a fixed-wing aircraft, scanning at a 600 kHz target pulse rate. The maximum survey altitude was 2286 m with a target aircraft speed of approximately 240 km/h. The maximum scan angle was 18° off nadir with at least a 55 % swath-to-swath overlap. Range data from the lidar sensor were processed into LAS format using the Optech Lidar Management Suite. The point density using all returns on the field plots was 16.8 pts/$m^2$ and the point density for ground returns was 1.6 pts/$m^2$. Intensity values for each return were dynamically normalized by the vendor. Ground points were used to develop a digital terrain model approximately 0.3 m in resolution, which was then used to create elevation-normalized point clouds used for further analysis. These lidar data are publicly available through the 3D Elevation Program of the United States Geological Survey, who provided funding for the Oregon Department of Forestry for the acquisition.

We generated lidar predictors for each field plot by overlaying a set of rasterized lidar values. The normalized point clouds were first rasterized into 20 m grid cells by computing a suite of summary statistics for lidar heights in each grid cell. The first group of summary statistics encapsulated vertical structural information, including height percentiles (5th, 30th, 80th, 95th), the mean height, and the coefficient of variation of height. The second group of summary statistics encapsulated information about the lidar intensity values, including intensity percentiles (5th, 30th, 80th, 95th), the mean intensity, and the coefficient of variation of intensity. Lidar intensity values quantify the reflectance properties of surfaces that intercept the lidar pulse, and has demonstrated utility in discriminating between live and dead trees (Bright et al., 2013). These summary statistics were applied to two distinct strata within each cell, referred to as the canopy and subcanopy strata. The canopy stratum composed the set of points exceeding 2 m, and the subcanopy stratum contained all other points. Together, 12 predictors were calculated for the canopy and subcanopy strata, for a total of 24 predictors. Finally, we calculated a cover index, which is the number of points in the canopy stratum divided by the total number of points, for a total of 25 lidar predictors (Table 2). The rasterized lidar predictors were then overlayed with the field plot footprints, which are composed of four 7.3 m subplots. To calculate a plot-level predictor value, the weighted mean of the rasterized pixel values that intersect the plot shape was taken, where the weights arose from the fraction of each pixel that covers the plot shape after the intersection. This is referred to as a "raster-intersect" approach which, combined with a 20 m raster resolution, was found to be a robust option for clusters of circular plots, like the FIA plot configuration, in a recent study (Strunk et al., 2025).

**Table 2**
Lidar and DAP predictors used in the regression models. With the exception of cover, each covariate is calculated for the set of two strata: points falling above 2 m (canopy points) and the set of points falling below 2 m (subcanopy points).

| Source | Covariate Name | Description |
|---|---|---|
| Lidar and DAP | z_p5 | 5th percentile height |
| | z_p30 | 30th percentile height |
| | z_mean | Mean height |
| | z_p80 | 80th percentile height |
| | z_p95 | 95th percentile height |
| | z_cv | Coefficient of variation of height |
| | cover | Number of canopy returns divided by total returns |
| Lidar Only | int_p5 | 5th percentile intensity |
| | int_p30 | 30th percentile intensity |
| | int_mean | Mean intensity |
| | int_p80 | 80th percentile intensity |
| | int_p95 | 95th percentile intensity |
| | int_cv | Coefficient of variation of intensity |

### 2.3.2. Digital aerial photogrammetric point clouds

A digital aerial photogrammetric (DAP) point cloud was derived from 2022 leaf-on digital imagery collected via fixed-wing aircraft during the Summer of 2022 collected by Hexagon as part of a statewide NAIP acquisition. The flying height of the aircraft averaged 4470 m, yielding a nominal ground sample distance of 15 cm. The collection used the Leica Geosystem ContentMapper frame camera sensor, which collected red, green, blue, and near-infrared bands. Photogrammetric point clouds were derived using HxMap Infocloud software by analysts from the remote sensing vendor Hexagon. The software uses the semi-global matching algorithm to infer pixel elevations from stereo image pairs. The software provides coordinates (in three-dimensional space) and red, green, blue, and near infrared values for each point. The point density on the field plots was 13.9 pts/$m^2$. We did not use the spectral information owing to topographic effects. Instead, we used reflectance data from Sentinel-2, a sensor that includes shortwave infrared bands, enabling calculation of fire effects indices such as the normalized burn ratio (Section 2.3.3). Our workflow generated several rasterized predictors summarizing the vertical distribution of points:

1. Point clouds were normalized using the lidar-generated DTM;
2. Predictors were calculated for each 20 m grid cell, such that the resultant rasters aligned with Sentinel-2 images. Note that the DAP predictors only included height statistics, because the DAP data lacked intensity, and other multispectral information was unsuitable due to topographic anomalies;
3. As with lidar data, height statistics were produced for canopy (points with heights greater than two meters) and subcanopy (heights less than or equal to two meters) strata.

Rasters for both the DAP and lidar point clouds were produced using the *lidR* software package (Roussel et al., 2020) in the R programming language (Core Team, 2024).

### 2.3.3. Sentinel-2 imagery

A pair of Sentinel-2 images collected in Summer, 2019 (pre-fire) and Summer, 2022 (post-fire), were obtained from the Level-2A orthorectified and atmospherically corrected surface reflectance collection on Google Earth Engine. The post-fire image year of 2022 was used to align with the acquisition dates of the DAP and lidar point clouds (Table 3). Vegetation indices, such as the normalized difference vegetation index (NDVI), and others, are commonly used as predictors for forest inventory attributes (e.g., Moradi et al., 2022; Zhou and Feng, 2023) and for studying wildfire effects (e.g., Meng et al., 2017). Tasseled cap transformations, specifically brightness and wetness, have proved useful for discriminating between salvage logging areas and burned areas (Li

**Table 3**
A description of remote sensing data sources used in the study and their collection dates. For the DAP and lidar sources, the collection dates are given as a duration between the starting and ending dates over the study region.

| Data Source | Collection Date(s) |
|---|---|
| DAP | 11 July 2022–8 August 2022 |
| Lidar | 17 August 2022–7 September 2022 |
| Sentinel-2 Pre-fire Image | 12 June 2019 |
| Sentinel-2 Post-fire Image | 7 July 2022 |

and Xu, 2023), both of which were prevalent in our study region. We calculated various vegetation indices, fire effects indices, and tasseled cap transformations described in Table 4. All indices calculated for the post-fire scene were included as predictors, along with differenced indices, referred to by the prefix “d” (e.g., dNDVI), calculated relative to the pre-fire scene.

## 3. Methods

### 3.1. Post-fire forest attribute regression models

In this analysis we relied on nonparametric regression techniques and adopted a mode of statistical inference that is common with nonparametric methods. The sample data were $n$ pairs of response variables, $y_i$, and vectors of predictors, $\boldsymbol{x}_i$. A random forest model fitted to a sample of observations allowed predictions of the attribute of interest at any location, provided the predictors were available, and rendered predictive forest inventory maps. We used random forest to obtain model fits with the specific implementation given in the R package *ranger* (Wright and Ziegler, 2017). Random forest is well suited for predictive modeling tasks, especially when nonlinearity and complex interactive effects among the predictors are present and when *a priori* knowledge of the functional form of the trend is limited. We fit random forest models for pairs of predictor sets, which are collections of predictors formed from different remote sensing sources, and the forest attributes of interest. In total, we considered five predictor sets, representing lidar only, DAP only, Sentinel-2 only, lidar combined with Sentinel-2, and DAP combined with Sentinel-2. Each predictor set was paired with each of the four forest attributes of interest (Section 2.2), yielding 20 predictive models. A workflow diagram of the data processing and modeling steps is given in Fig. 2.

### 3.2. Performance measures

To compare performances among the random forest models, we used leave-one-out cross-validation, which can be used to estimate the root mean square error, bias, and coefficient of determination for models fit on new data drawn from the population (Bates et al., 2024). Let $\widehat{y}_i$ refer to the predicted value of plot $i$ for a random forest fit made with the $i$th plot left out. We obtain the leave-one-out cross-validation estimate of the root mean square error

$$RMSE = \sqrt{\frac{1}{n}\sum_{i=1}^{n}(y_i - \widehat{y}_i)^2} \tag{1}$$

where $y_i$ is the observed value for plot $i$ and $n$ is the sample size. Next, we obtain an estimate of the bias

$$Bias = \frac{1}{n}\sum_{i=1}^{n}(y_i - \widehat{y}_i) \tag{2}$$

and an estimate of the coefficient of determination

$$R^2 = 1 - \frac{\sum_{i=1}^{n}(y_i - \widehat{y}_i)^2}{\sum_{i=1}^{n}(y_i - \overline{y})^2} \tag{3}$$

where $\overline{y}$ is the sample mean. In addition to the performance measures in (1-3), we also produce estimates of the relative RMSE and relative bias by dividing each by the sample mean for the attribute of interest.

To compare the performances of models that use DAP versus lidar predictors we calculated a percentage difference in RMSE. We obtain

$$dRMSE\% = \frac{RMSE - RMSE'}{RMSE'} \cdot 100 \tag{4}$$

where $RMSE'$ refers to a fit using a predictor set different from $RMSE$. In particular, $RMSE$ represents a random forest model fit using DAP (e.g., DAP with or without Sentinel-2), and $RMSE'$ represents a model fit using lidar (e.g., lidar with or without Sentinel-2). For example, the value of $dRMSE\%$ exceeds zero when the DAP model has a larger root mean square error than the lidar model.

### 3.3. Variable importance

Remote sensing studies that use the random forest algorithm often report variable importance, which can be used to identify predictors that result in reduced error when included in the model. In the presence of highly correlated predictors, variable importance estimates from the random forest implementation we use are deflated (Wright and Ziegler, 2017; Hooker et al., 2021). We eliminated predictors that exceeded correlation coefficients of 0.95 when paired with another predictor. The predictors EVI and SAVI were found to be highly correlated with MSAVI, and the differenced predictors dEVI and dSAVI were highly correlated

**Table 4**
Descriptions and references for post-fire Sentinel-2 vegetation indices used in the regression models.

| Covariate Name | Description | Reference | Difference Acronym |
|---|---|---|---|
| Normalized Burn Ratio (NBR) | $\frac{\mathrm{NIR} - \mathrm{SWIR}_2}{\mathrm{NIR} + \mathrm{SWIR}_2}$ | Key and Benson (2005) | dNBR |
| Relative Differenced Normalized Burn Ratio (RdNBR) | $\frac{\mathrm{dNBR}}{\sqrt{\lvert \mathrm{NBR}_{\mathrm{Pre}} \rvert}}$ | Miller et al. (2009) | – |
| Normalized Difference Vegetation Index (NDVI) | $\frac{\mathrm{NIR} - \mathrm{R}}{\mathrm{NIR} + \mathrm{R}}$ | Tucker (1979) | dNDVI |
| Excess Green Index (EGI) | $2\mathrm{G} - \mathrm{R} - \mathrm{B}$ | Woebbecke et al. (1995) | dEGI |
| Burned Area Index (BAI) | $\left((0.1 - \mathrm{R})^2 + (0.06 - \mathrm{NIR})^2\right)^{-1}$ | Chuvieco et al. (2002) | dBAI |
| Modified Soil Adjusted Vegetation Index (MSAVI) | $\frac{2\mathrm{NIR} + 1 - \sqrt{(2\mathrm{NIR} + 1)^2 - 8(\mathrm{NIR} - \mathrm{R})}}{2}$ | Qi et al. (1994) | dMSAVI |
| Tasseled Cap Brightness (TCB) | $b_1\mathrm{B} + b_2\mathrm{G} + b_3\mathrm{R} + b_4\mathrm{NIR} + b_5\mathrm{SWIR}_1 + b_6\mathrm{SWIR}_2$ | Shi and Xu (2019) | dTCB |
| Tasseled Cap Greenness (TCG) | $g_1\mathrm{B} + g_2\mathrm{G} + g_3\mathrm{R} + g_4\mathrm{NIR} + g_5\mathrm{SWIR}_1 + g_6\mathrm{SWIR}_2$ | Shi and Xu (2019) | dTCG |
| Tasseled Cap Wetness (TCW)* | $w_1\mathrm{B} + w_2\mathrm{G} + w_3\mathrm{R} + w_4\mathrm{NIR} + w_5\mathrm{SWIR}_1 + w_6\mathrm{SWIR}_2$ | Shi and Xu (2019) | dTCW |

Note: Sentinel-2 bands are referred to by their acronyms, near infrared (NIR), the first shortwave infrared band (1610.4 nm, SWIR1), the second shortwave infrared band (2202.4 nm, SWIR2), red (R), green (G), and blue (B). Coefficient values for tasseled cap indices are provided in the supplementary material.

 

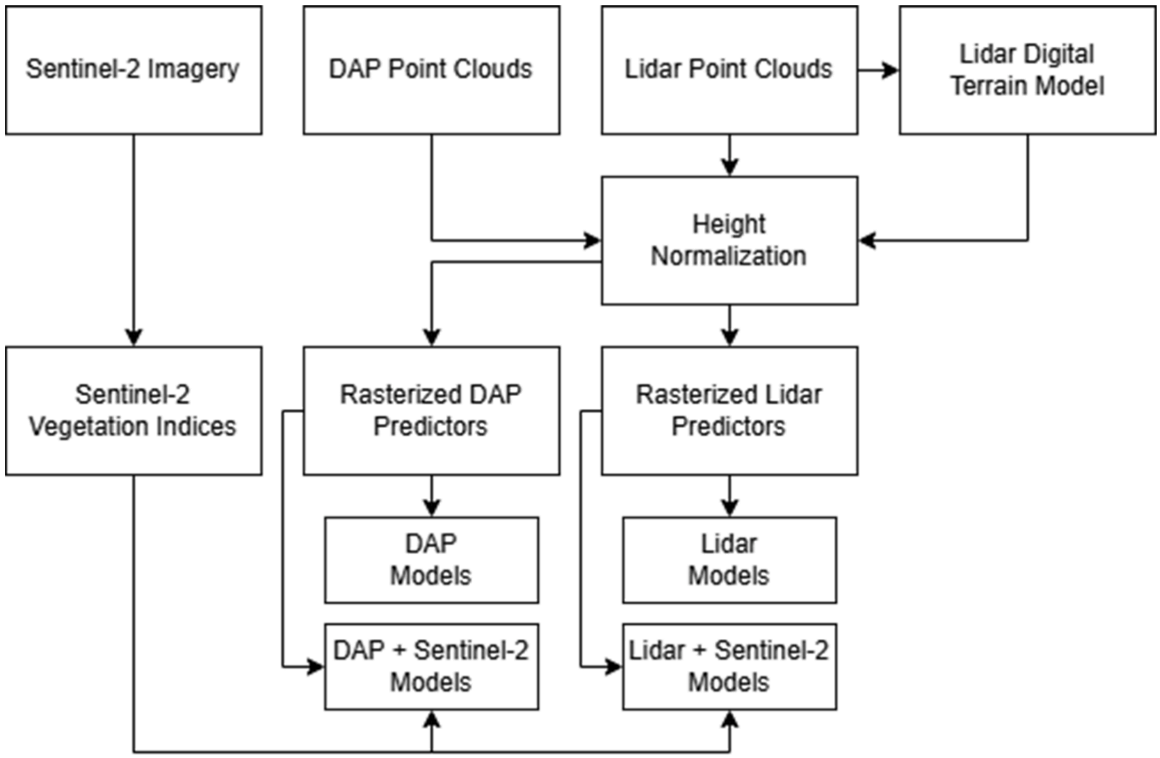


**Fig. 2.** A workflow diagram specifying the steps used to create forest attribute models.

with dMSAVI. Accordingly, MSAVI and dMSAVI were retained and EVI, SAVI, dEVI, and dSAVI were discarded. Additionally, the 80th percentile canopy lidar and DAP height predictors and the 80th percentile canopy lidar intensity predictor were removed due to high correlations with mean canopy height and mean canopy intensity, respectively. Ultimately, within a model, variable importances were scaled over the sum of the variable importances for all predictors in the model and multiplied by 100, which we refer to as the variable importance in percent.

### *3.4. Accumulated local effects*

In this analysis, it is desirable to understand how the predictors influence the prediction model for a given attribute, which can elucidate potential biophysical processes that dictate the behavior of the model. To help further understand the nature of the associations between various remote sensing predictors and post-fire forest attributes, we used the emerging visualization tool referred to as accumulated local effect plots (ALEs hereafter; Apley and Zhu, 2020). ALEs are a graphical representation of how predictors influence predictions and are a way to examine the behavior of complex prediction functions like random forest. A line is used to demonstrate the relationship between the prediction and different values of the predictor. The graphical representation can be used to identify values of the predictor that cause the model prediction to increase or decrease relative to the mean, which is recentered at zero. Steeper slopes in the ALE represent values of the predictors that have a strong influence on the prediction behavior within a local region of the predictor space. We used the R package *iml* to calculate the accumulated local effects (Molnar et al., 2018).

### *3.5. Exploration of canopy height discrepancies*

Canopy heights derived from three-dimensional data sources are often the primary predictors in forest attributes of interest. Upon an initial graphical inspection of the DAP and lidar data sources in this study, stark differences in canopy heights were apparent in many areas within the fire perimeter, motivating explicit exploration of the processes driving these disagreements. We used a random forest model to explain discrepancies in height between the two remote sensing products expressed as a ratio. We defined the height ratio as

$$r_i = \frac{x_{i,p95,DAP}}{x_{i,p95,Lidar}} \tag{5}$$

where $x_{i,p95,DAP}$ is the DAP 95th percentile canopy height and $x_{i,p95,Lidar}$ is the lidar 95th percentile canopy height for the *i*th pixel. Then, the height ratio values were used as a response variable in a random forest model that uses all previously defined lidar and Sentinel-2 predictors as covariates (Section 2.3). Because the height ratio does not require any field information, we formed a sample of pixels selected within the fire perimeter using simple random sampling without replacement of an initial sample size of 10,000 pixels. Pixels with no lidar points in the canopy stratum imply a zero in the denominator of the height ratio and were discarded from the sample. These pixels generally represent bare ground areas. Height ratio values exceeding two were also discarded from the sample after visual inspection of height ratio values confirmed that they generally represented areas that contained no trees or were harvested between the DAP and lidar collection dates, respectively. The variable importance is used as defined previously (Section 3.3) to identify explanatory variables that drove the height discrepancies between DAP and lidar. The leave-one-out RMSE and $R^2$ performance measures were estimated using a random subsample of 500 pixels selected with simple random sampling without replacement for computational convenience.

## 4. Results

### *4.1. Performances of DAP and lidar post-fire models*

Several performance measures were used to compare lidar, DAP, and Sentinel-2 driven models in the prediction of post-fire forest attributes. Lidar predictors explained the most variation in all four post-fire forest attributes (Table 5). The inclusion of Sentinel-2 with lidar was only

**Table 5**
Summary of cross-validated model performances for all post-fire forest attributes models in the analysis: live aboveground biomass (LAGB), standing dead aboveground biomass (DAGB), live stem density (LDEN), and relative basal area change (RBAC) for the predictor sets: Sentinel-2, DAP, DAP + Sentinel-2, lidar, and lidar + Sentinel-2.

| Predictor Set | Attribute | Bias | RMSE | $R^2$ | Attribute | Bias | RMSE | $R^2$ |
|---|---|---|---|---|---|---|---|---|
| Sentinel-2 | LAGB | -17 (−17 %) | 127 (123 %) | 0.41 | LDEN | -11 (-8 %) | 182 (137 %) | 0.31 |
| DAP | LAGB | 1 (1 %) | 88 (85 %) | 0.72 | LDEN | -2 (-2 %) | 188 (141 %) | 0.26 |
| DAP + Sentinel-2 | LAGB | -2 (-2 %) | 86 (83 %) | 0.73 | LDEN | -6 (-4 %) | 179 (135 %) | 0.33 |
| Lidar | LAGB | -1 (-1 %) | 79 (76 %) | 0.77 | LDEN | -13 (-10 %) | 173 (130 %) | 0.38 |
| Lidar + Sentinel-2 | LAGB | -3 (-3 %) | 84 (81 %) | 0.74 | LDEN | -9 (-7 %) | 171 (129 %) | 0.39 |
| Sentinel-2 | DAGB | -17 (-16 %) | 91 (85 %) | 0.45 | RBAC | 0 (0 %) | 0.32 (58 %) | 0.42 |
| DAP | DAGB | -20 (-18 %) | 108 (100 %) | 0.22 | RBAC | -0.03 (-6 %) | 0.31 (58 %) | 0.43 |
| DAP + Sentinel-2 | DAGB | -11 (−10 %) | 88 (81 %) | 0.48 | RBAC | -0.01 (-1 %) | 0.29 (54 %) | 0.51 |
| Lidar | DAGB | -5 (-5 %) | 75 (69 %) | 0.62 | RBAC | 0 (0 %) | 0.26 (47 %) | 0.62 |
| Lidar + Sentinel-2 | DAGB | -8 (-8 %) | 76 (71 %) | 0.60 | RBAC | 0 (-1 %) | 0.27 (50 %) | 0.58 |

marginally helpful, with a maximum increase in $R^2$ of only 0.04 for relative basal area change. DAP explained much less variation in the four post-fire attributes than lidar and was only marginally helpful in the prediction of standing dead aboveground biomass and live stem density over the standalone Sentinel-2 model. For live aboveground biomass and relative basal area change, the combined DAP and Sentinel-2 models were more effective than either data source alone. In general, models that used either DAP or lidar exhibited absolute relative biases less than or equal to 10 %, with the standalone DAP standing dead aboveground biomass model as a notable exception which exhibited severe overprediction behavior (-18 % relative bias). Standalone Sentinel-2 models also exhibited absolute relative biases exceeding 10 % for live aboveground biomass, and standing dead aboveground biomass, and had similar overprediction behavior (-17 % and -16 % for the live aboveground biomass and standing dead aboveground biomass Sentinel-2 models, respectively). In most cases, lidar models were dramatically better than models that used other auxiliary data sources, with smaller biases and RMSEs.

The relative performances of lidar and DAP models are often very different for a given forest attribute. In general, standalone lidar models tend to clearly outperform standalone DAP models. This divergence in performance is captured by the percent difference in root mean square error (dRMSE%), which quantifies the change in RMSE when exchanging DAP data with lidar data for a given forest attribute (Table 6). The largest percent difference in RMSE for models that did not utilize Sentinel-2 was 46.9 % for standing dead aboveground biomass, followed by relative basal area change (22.2 %), live aboveground biomass (11.3 %), and live stem density (9.8 %). However, augmenting the point cloud sources with Sentinel-2 markedly reduced these discrepancies, with standing dead aboveground biomass obtaining the largest reduction, followed by relative basal area change, live aboveground biomass, and finally live trees per hectare. Models of live aboveground biomass and live trees per hectare achieve very similar levels of mean square error, with percent differences in RMSE less than 5 percent. Observed versus predicted plots are given in Fig. 3.

### 4.2. Prediction model behavior

Identifying the drivers of prediction model behavior can elucidate potential biophysical factors that explain the outcome of the regression model. For this purpose, we examined both variable importance and accumulated local effects plots. We used a rescaled variable importance measure that quantifies the importance of each predictor used in a given regression model and enables comparisons of importance across multiple attributes. Analyses of variable importance and accumulated local effects were focused on the DAP + Sentinel-2 models and Lidar + Sentinel-2 models as they are the most likely to be implemented in practice.

**Table 6**
Percent differences in RMSE between DAP and lidar models for each forest attribute. Values of dRMSE% that are larger than zero indicate a larger DAP model root mean square error.

| Attribute | dRMSE% without Sentinel-2 | dRMSE% with Sentinel-2 |
|---|---|---|
| LAGB | 11.3 % | 3.0 % |
| DAGB | 46.9 % | 16.1 % |
| LDEN | 9.8 % | 4.8 % |
| RBAC | 22.2 % | 7.7 % |

Lidar + Sentinel-2 models used different predictors for each of the four forest attributes. Importance of lidar canopy height and cover predictors tended to be high for all attributes relative to other predictors, except for relative basal area change (Fig. 4). Intensity predictors were unique to the lidar dataset, and these predictors were of moderate to high importance for all four attributes we investigated. Notably, subcanopy intensity percentiles and the subcanopy coefficient of variation were highly important for live aboveground biomass, while canopy intensity percentiles were important for live stem density and relative basal area change. Sentinel-2 predictors tended to be less important than intensity and structural predictors. NBR and dNBR were both important for standing dead aboveground biomass and relative basal area change, respectively. Sentinel-2 variable importance values were all less than 5 % for the live aboveground biomass and live stem density models.

DAP + Sentinel-2 models also varied in variable importance across forest attributes. Sentinel-2 information was relatively unimportant when predicting live aboveground biomass, and the model relied heavily instead on canopy height information (Fig. 4). In contrast, the model for standing dead aboveground biomass tended to rely almost entirely on Sentinel-2 predictors, especially dNBR, with approximately 10 % more of the variable importance than any other variable. Live stem density differed from both live aboveground biomass and standing dead aboveground biomass in that cover is more important than other attributes. For relative basal area change, NBR, dNBR, and RdNBR were the most important predictors, while structural predictors from DAP were relatively unimportant. There were some clear differences in variable importance between DAP and lidar. The Lidar + Sentinel-2 models relied more on structural predictors than the DAP models for some attributes (Fig. 4). For example, canopy height predictors were some of the most important variables when predicting standing dead aboveground biomass from lidar. For DAP + Sentinel-2 models, in contrast, Sentinel-2 information played a stronger role in standing dead aboveground biomass models. For lidar, subcanopy and canopy intensity values were important predictors, especially for live aboveground biomass, live stem density, and relative basal area change. These differences between DAP and lidar reflect some fundamental differences between these technologies: lidar provides structure information about the subcanopy and has intensity data, while DAP generally does not provide subcanopy structure, often misses lone trees, and, in our study, did not provide any information that was analogous to intensity.

Accumulated local effects plots provided insight into how models use predictors to make predictions of each attribute. ALE plots for the DAP +

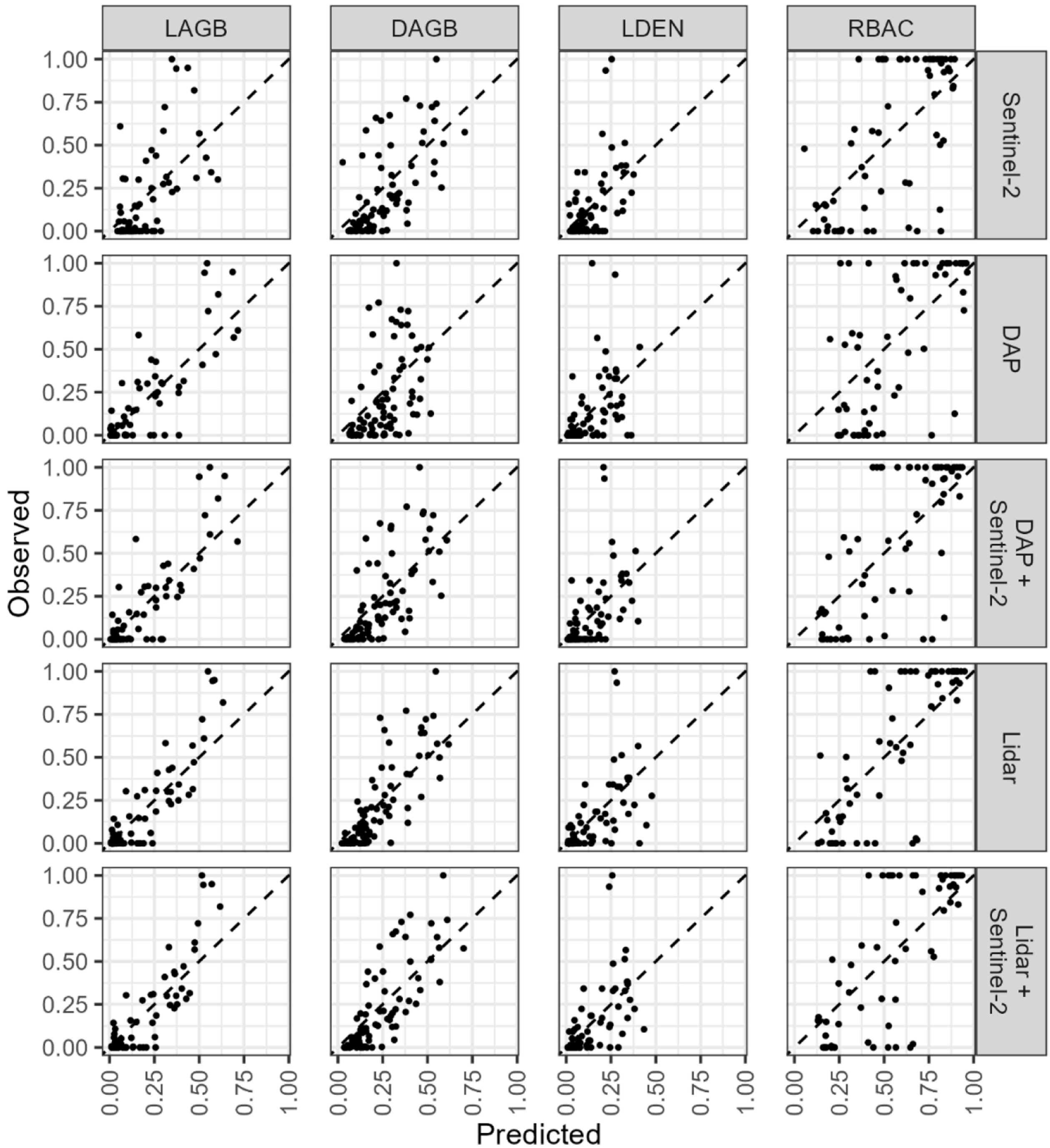


**Fig. 3.** Predicted vs. observed plots for live aboveground biomass (LAGB), standing dead aboveground biomass (DAGB), live stem density (LDEN), and relative basal area change (RBAC) models, each using predictors from either Sentinel-2, DAP, lidar, or lidar and DAP augmented with Sentinel-2. Note that the data are scaled to the [0, 1] interval to facilitate comparisons.

Sentinel-2 and Lidar + Sentinel-2 models are provided together for a set of predictors which had relatively large importance values in at least one model (Fig. 5). ALE plots for the DAP + Sentinel-2 and Lidar + Sentinel-2 models indicated that these two sources of information have similar relationships to post-fire forest attributes, with some clear distinctions. For example, the shape of the ALEs for cover between DAP and lidar models strongly resembled each other for the live aboveground biomass and live stem density attributes, albeit their locations were somewhat mismatched. The steepest parts of an ALE trend indicate values of the predictors that impart large changes in the predicted value for that model. In the case of cover for these two attributes, lidar predictions rapidly increased at approximately 50 % (lidar) cover, while DAP predictions rapidly increased at 75 % (DAP) cover. However, the overall shapes of the ALEs in these two cases were similar, suggesting that the DAP and lidar models used cover information in similar ways. For example, smaller values of cover drive larger predictions of relative basal area change, suggesting an increase in predicted fire severity when cover values are small. Similar trends were observed in the other attributes, including 95th percentile canopy height and dNBR. The overall slope of each ALE is an indicator of how sensitive the model predictions are to different values of the predictor. Notably, the slopes of the ALEs for dNBR within the lidar model tended to be less steep, which reflects the lower importance we observed earlier (Fig. 4). Intensity predictors played a large role in predicting live aboveground biomass and relative

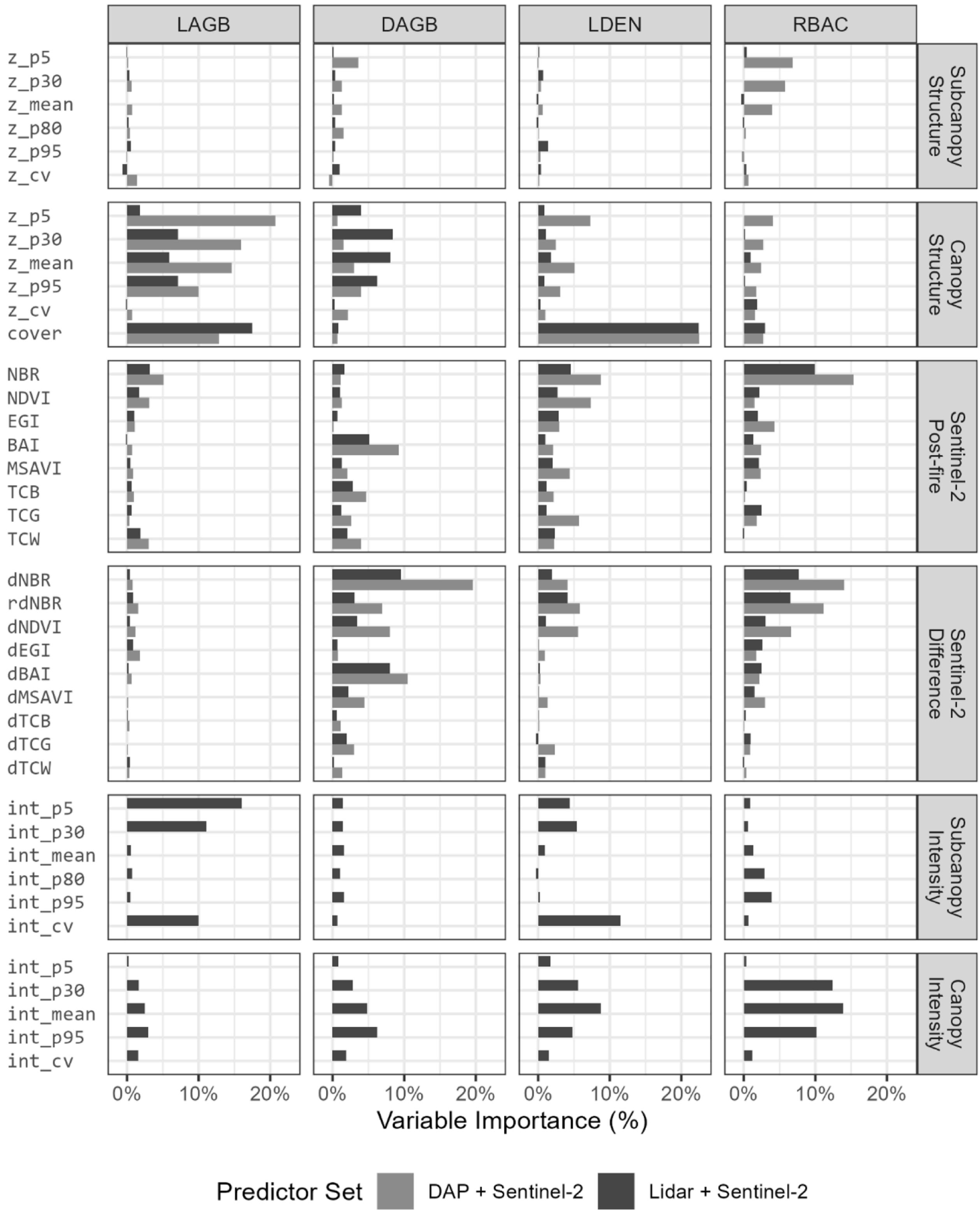


**Fig. 4.** Variable importance for each predictor used in the post-fire predictive models for the DAP + Sentinel-2 and Lidar + Sentinel-2 predictor sets. Facet columns represent the different forest attributes, and facet rows represent the different predictor types. The attributes are live aboveground biomass (LAGB), standing dead aboveground biomass (DAGB), live stem density (LDEN), and relative basal area change (RBAC).

basal area change. As the 5th percentile subcanopy intensity increases past values of 50, the ALE indicates that the live aboveground biomass model drastically reduces predictions downward relative to the mean. Similarly, as the mean canopy intensity increases past values of 100, the ALE indicates that the relative basal model drastically reduces predictions downward relative to the mean.

The fitted models in this analysis were used to create predictive maps for each forest attribute. Fig. 6 displays the mapped predictions for all attributes for the DAP + Sentinel-2 and Lidar + Sentinel-2 models. When inspecting the relative basal area change maps as a measure of fire

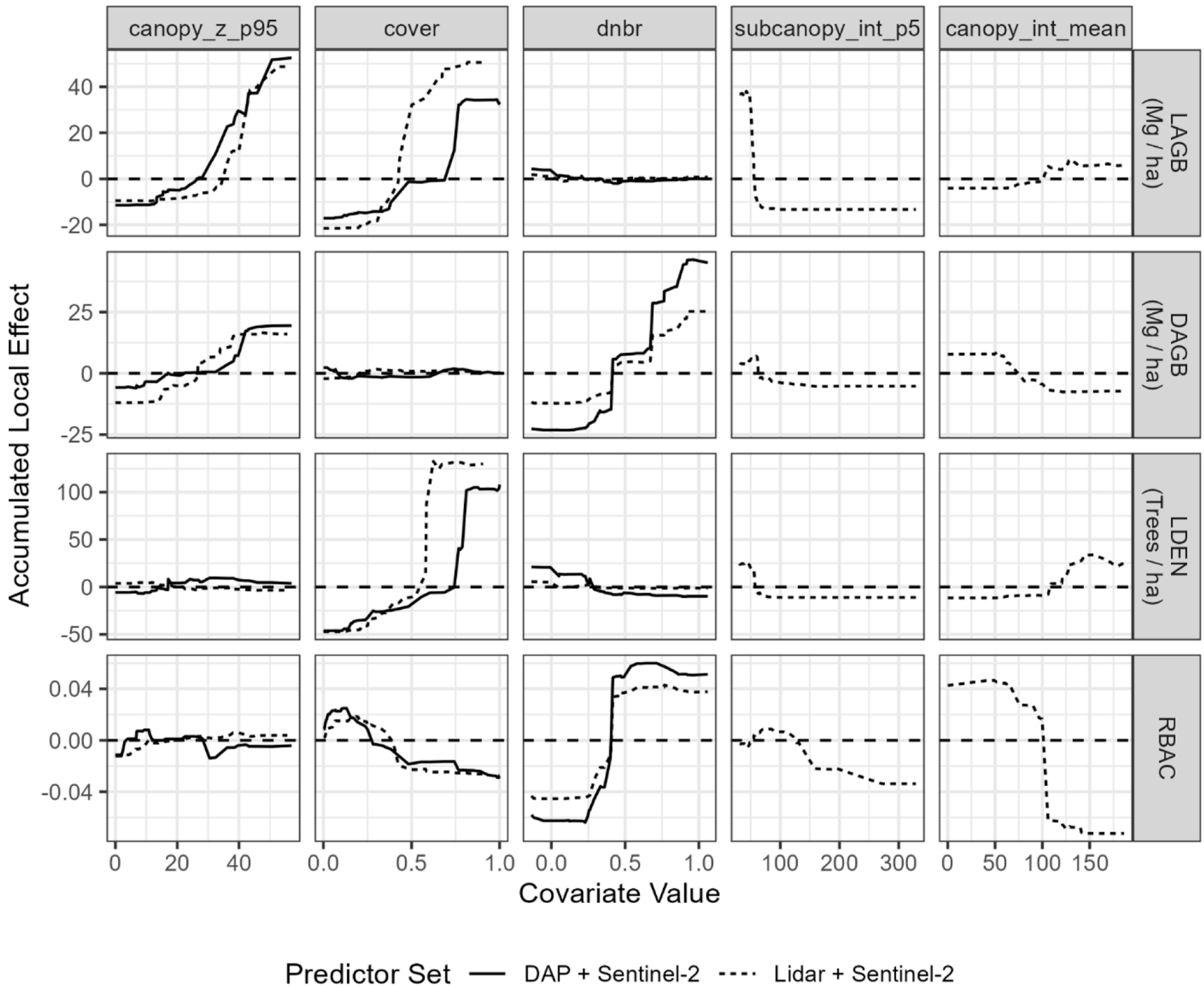


**Fig. 5.** Accumulated local effects for a subset of five predictors used in the augmented Sentinel-2 live aboveground biomass (LAGB), standing dead aboveground biomass (DAGB), live stem density (LDEN) and relative basal area change (RBAC) models.

severity, it is apparent that the highest severity portion of the fires were in the central western portion of the Beachie Creek fire and the majority of the Lionshead fire. In contrast, the far western portion of the Beachie Creek fire burned primarily at moderate to low severity after high winds abated, and also exhibited patterns of forest management activity, with clearly identifiable cut blocks in the northwestern and southwestern fingers of the fire in the live aboveground biomass maps. Visually, the mapped predictions for each attribute generated from each predictor set appear to be highly similar, which is further supported by the similarities in the observed versus predicted plots discussed previously (Fig. 3). We also obtained maps of differences between the DAP + Sentinel-2 and Lidar + Sentinel-2 models for each forest attribute (Fig. 7), which depict areas exhibiting strong disagreement. In general, large disagreements were evident for each of the four attributes, with the most extreme differences seen when live aboveground biomass and standing dead aboveground biomass exceeded 100 Mg·ha$^{1}$, in live stem density when it exceeded 100 trees per hectare, and in relative basal area change when it exceeded 0.2. Standing dead aboveground biomass exhibits large positive and negative differences in areas of high fire severity, i.e., the center west and eastern portions of the study region, with smaller differences in the western fingers. The other three attributes exhibited mixed patterns, with substantial positive and negative differences distributed throughout the study region. Some islands of extreme positive differences for all four attributes (i.e., lidar predicted greater values than DAP) exist in the southern portion of the Lionshead fire, which were ultimately explained by post-fire salvage harvest having occurred between the lidar and DAP acquisitions.

### 4.3. Discrepancies in lidar and DAP canopy height

Canopy heights are often the leading predictors in forest attribute models that use lidar or DAP data. In the previous section, we observed that canopy height predictors tended to obtain higher variable importance values in lidar models than in DAP models (Fig. 4). Generally, canopy height predictors derived from lidar are considered to be some of the highest quality auxiliary information related to tree heights, second only to direct measurements from the field (e.g., Andersen et al., 2006). Thus, deviations from lidar canopy height predictors when adopting DAP as an alternative are important to consider. We investigated the ratio of the 95th percentile DAP canopy height to the 95th percentile lidar height, i.e., the height ratio, using a random forest model trained on a large sample obtained directly from the rasterized lidar and Sentinel-2 data sets (Section 4.2). The purpose of this model was to identify predictors that explained the height ratio, which can lend insight into potential pitfalls for using DAP as an alternative to lidar in post-fire environments.

Variable importance values for the height ratio model revealed drivers in disagreement between DAP and lidar canopy height predictors. The five most important predictors for explaining the height ratio are given in Table 7. Lidar cover had the highest variable

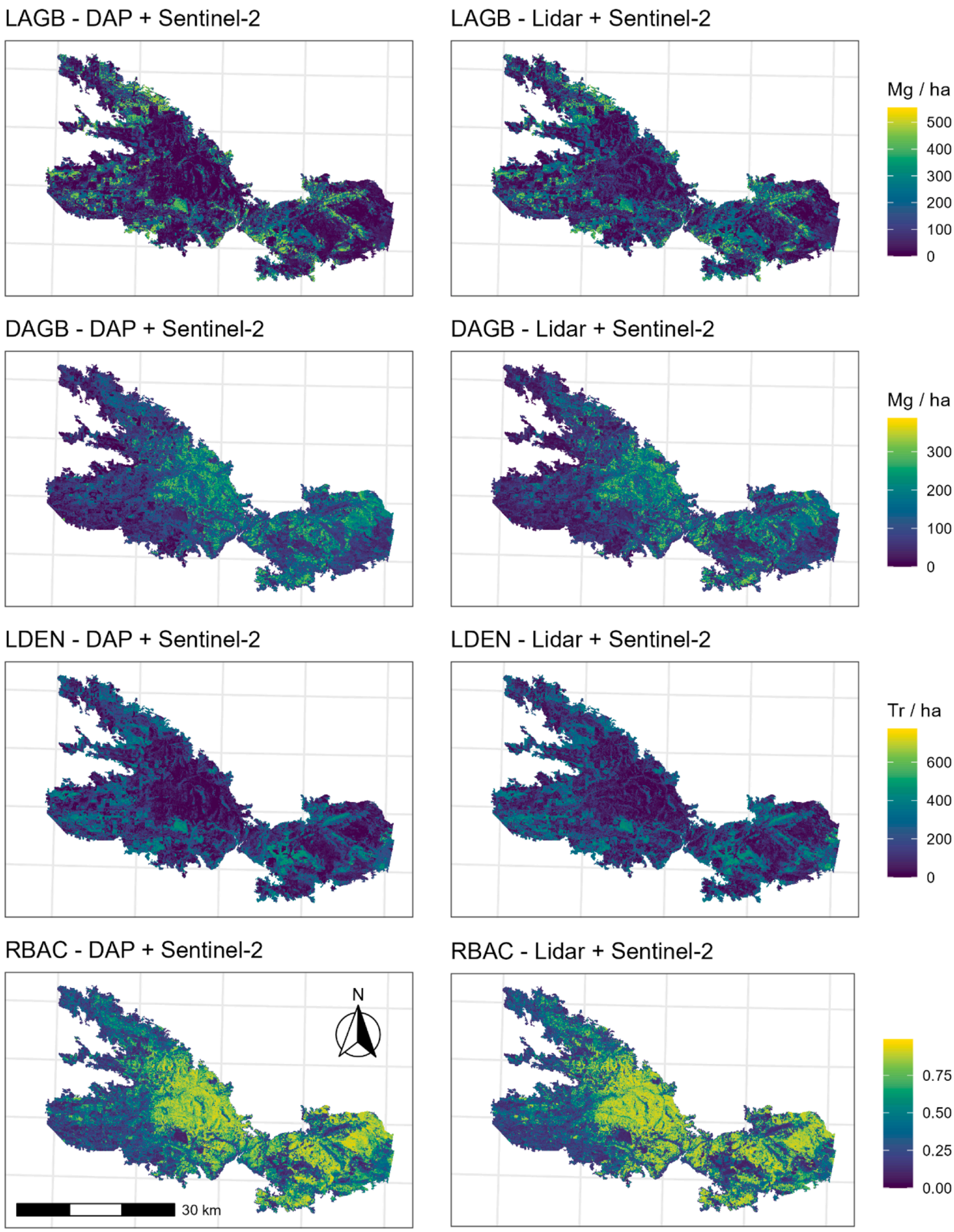


**Fig. 6.** Maps of forest attribute predictions for live aboveground biomass (LAGB), standing dead aboveground biomass (DAGB), live stem density (LDEN), and relative basal area change (RBAC) for the DAP + Sentinel-2 and Lidar + Sentinel-2 models.

importance, followed by 95th percentile canopy intensity, mean canopy intensity, NBR, and 80th percentile canopy intensity. The height ratio model explained a large proportion of variation, with a cross-validated $R^2$ of 0.52. Fig. 8 depicts the true color Sentinel-2 post-fire image and the height ratio for a subset of the study region that experienced varying levels of fire severity. Darker blue colors in the height ratio map indicate locations where DAP height was much smaller than lidar height, and height ratios of zero often represent areas of total omission of trees in the DAP point cloud. Agreement between low values of lidar cover and high values in the height ratio map are apparent in Fig. 8, where high values of height ratio indicate the greatest disagreement between lidar and DAP. The greatest agreement occurs in the unburned and mixed severity areas in the southwestern corner of the image. The greatest disagreement occurs in areas of high severity fire and low canopy cover.

We looked more closely at the distributions of height ratios for lidar cover quintiles: non-overlapping 20 % intervals spanning from 0 % to

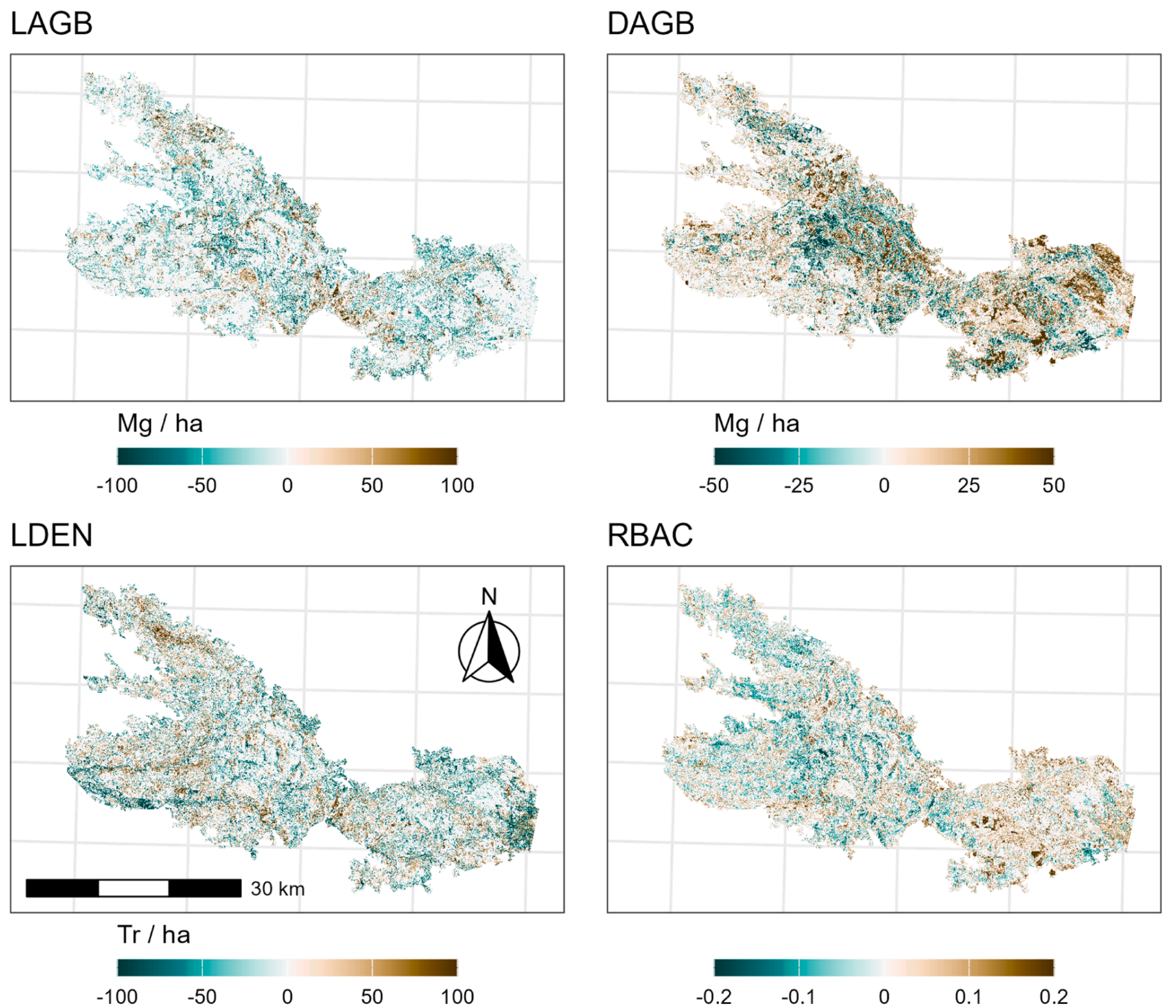


**Fig. 7.** Maps of differences between the DAP + Sentinel-2 and Lidar + Sentinel-2 predictions for live aboveground biomass (LAGB), dead aboveground biomass (DAGB), live stem density (LDEN), and relative basal area change (RBAC). Negative differences (cool colors) indicate areas where DAP + Sentinel-2 predictions are smaller than Lidar + Sentinel-2 predictions.

**Table 7**
Summary of the top five predictors ranked by variable importance, RMSE and $R^2$ for the height ratio random forest model. The relative RMSE is given in parentheses.

| Variable | Variable Importance (%) |
|---|---|
| Canopy_Cover | 9.5 % |
| Canopy_Int_p95 | 7.1 % |
| Canopy_int_mean | 7.1 % |
| NBR | 5.7 % |
| Canopy_Int_p80 | 5.3 % |
| RMSE | 0.22 (26 %) |
| $R^2$ | 0.52 |

100 %. The relationship between DAP and lidar heights decoupled for lidar cover values in the lower three quintiles, i.e., where canopy cover is less than 60 % (Fig. 9). While the median height ratio for the 40–60 % cover class was 0.99, the distribution was heavily skewed towards small (i.e., close to zero) values of height ratio. This suggests that omission of trees by DAP occurs in the 40–60 % cover class, and the discrepancy increases dramatically for 20–40 % and 0–20 % classes. Visual inspections of the DAP point clouds revealed many occurrences of tree omission. As an example, Fig. 10 displays lidar and DAP point clouds after height normalization for an area approximately 20 ha in size that experienced high fire severity. Visual inspection of post-fire orthophotos revealed all trees in this area were severely burnt, with no discernible live foliage. The omission of dead trees in the DAP relative to what was captured via lidar is apparent in the figure, and for areas like this one, the height ratio is close to zero. However, dead trees are not always fully omitted, and a strip of tree objects is apparent that crosses diagonally in the DAP point cloud, and represents areas where the height ratio is close to one. This example, combined with the wide distributions of height ratios given in Fig. 9, demonstrates that the omission of dead trees is not always uniform, creating an unreliable height signal for DAP in the presence of dead trees.

## 5. Discussion

### 5.1. *Relative performances of post-fire models*

Our analyses indicated that lidar is the single most powerful auxiliary data source for predicting the post-fire forest attributes we addressed. Still, some of the DAP models we investigated obtained very similar performances. For example, the DAP + Sentinel-2 models that quantified live vegetation, i.e., live aboveground biomass and live stem density, had percent differences in RMSE as small as 3.0 % and 4.8 %, respectively. In contrast, DAP + Sentinel-2 models were less successful relative to Lidar + Sentinel-2 models in predicting standing dead aboveground biomass and relative basal area change and had larger percent differences in RMSE of 16.1 % and 7.7 %, respectively. This is likely because DAP point clouds poorly capture individual trees,

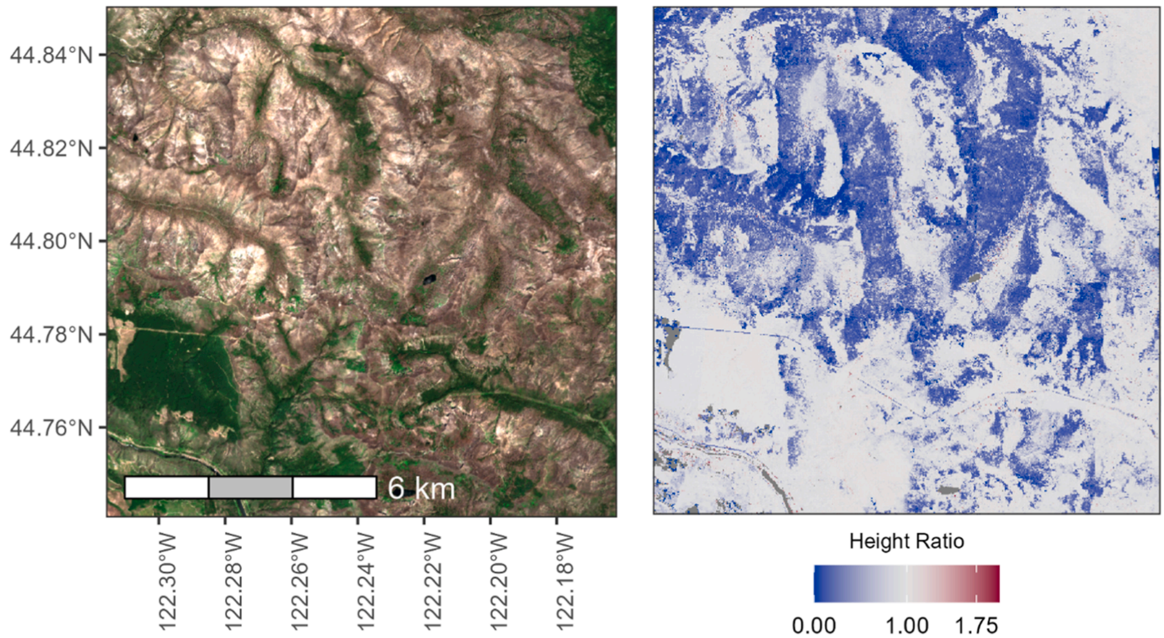


**Fig. 8.** Comparison of a post-fire Sentinel-2 image (left) and the ratio of DAP 95th percentile canopy height to lidar 95th percentile canopy height (right). White colors in the height ratio map represent high levels of agreement between the two canopy height predictors.

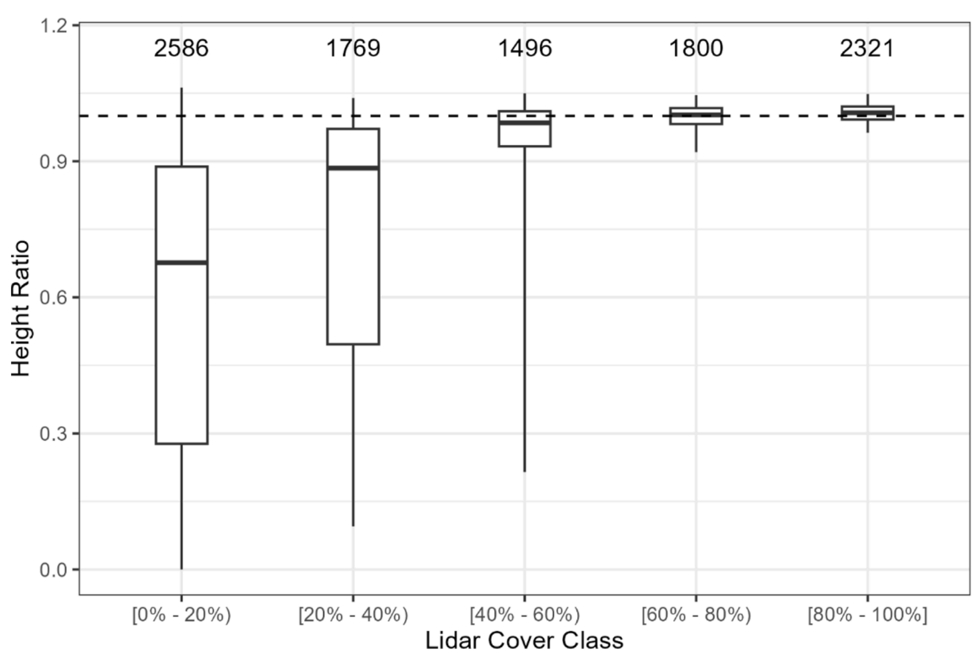


**Fig. 9.** Distribution of height ratios for five lidar cover classes. The horizontal lines within each box represent height ratio medians, hinges represent 25th and 75th percentiles, and whisker edges represent 5th and 95th percentiles. The dashed horizontal line indicates a height ratio value of one, which represents perfect agreement between lidar and DAP 95th percentile canopy height. Cover classes are indicated using interval notation, and the number of pixels in each cover class in the sample are given above each box.

particularly those devoid of live crowns. The large discrepancy in performance of the DAP + Sentinel-2 model relative to the Lidar + Sentinel-2 model for standing dead aboveground biomass was likely due to the decoupling of lidar and DAP 95th percentile heights in areas of low lidar cover (e.g., Figs. 8 and 9). In this study region, areas containing large stocks of standing dead aboveground biomass are those that experienced high fire severity and had large trees present before the fire. The Labor Day fires contained large portions of land that experienced crown fire (Busby et al., 2023), and we surmise that large amounts of canopy loss contributed to small values of post-fire lidar-detected post-fire canopy cover, which are associated with low quality DAP height predictors for these areas. With a less reliable signal in height predictors for DAP, the model was forced to rely on Sentinel-2 predictors instead, especially dNBR (Fig. 4), which did not directly capture correlates of tree biomass, such as height. This was the likely cause of saturation observed for DAP and Sentinel-2 in Fig. 3.

Inspection of observed versus predicted plots for all 20 models revealed systematic over-prediction for live aboveground biomass and live stem density, as indicted by the series of points falling along the bottom of the y-axis (Fig. 3). These points represent cases where live

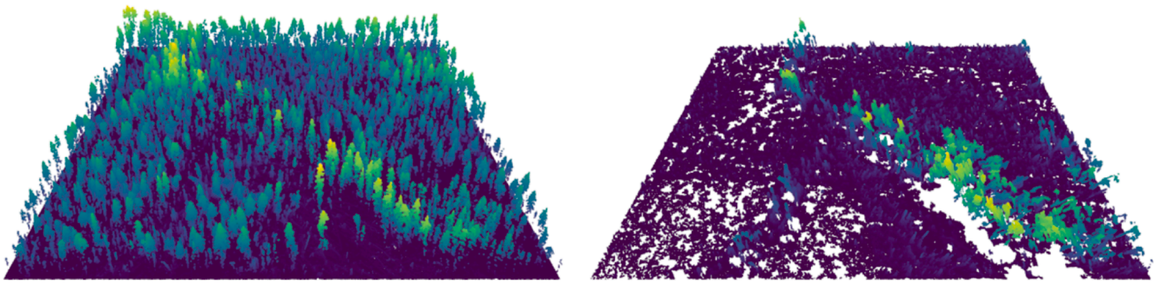

**Fig. 10.** Lidar (left) and DAP (right) point clouds for an area approximately 20 ha in size that experienced high fire severity. Photointerpretation of post-fire orthophotos was used to confirm that all trees in this area had no discernible live foliage. Points are colored by their height relative to ground.

trees larger than 12.7 cm at breast height were absent and correspond to areas that burned at high severity (Fig. 1). A similar, but less pronounced pattern was evident for plots with no standing dead aboveground biomass. Live stem density showed evidence of saturation as the maximum prediction was less than 50 % of what was observed. Models for relative basal area change were attenuated, with over-prediction of low values, and under-prediction of high values, evident from the linear point clusters falling along the bottom and top of the y-axis, respectively. Over-prediction on plots where live aboveground biomass is equal to zero may also result from new vegetation, e.g., shrubs or trees beneath the lower diameter limit of 12.7 cm growing between the dates of the fires and the field plot measurement date.

Several other studies have performed related analyses with comparable results. Our findings with respect to live aboveground biomass ($R^2$ up to 0.74) are in line with similar lidar-oriented studies for this geographic region by Sheridan et al. (2015) and Mauro et al. (2021). For live stem density, we observed relatively smaller coefficients of determination, between 0.26 and 0.39, across all DAP and lidar models than those observed by Strunk et al. (2020; $R^2$ from 0.40 to 0.45), in a geographically similar area. A distinction in our study was that the majority of our study area was burned, resulting in considerably lower canopy cover values, a condition that is particularly difficult for DAP. Strunk et al. (2020) examined a much larger pool of potential predictors, which may also have improved their results. Studies that evaluate relative basal area change are somewhat rare. An example by Hoe et al. (2018) had both pre- and post-fire lidar available for burn severity mapping, and their RMSE (0.12) was much smaller than that observed here (0.31). These differences are likely due to the availability of both pre- and post-fire lidar, but potentially also due to the higher mean relative basal area change observed in our study (0.57 here, versus ≈0.40 for their study, which was inferred from their relative RMSE%).

### 5.2. Implications for forest managers

Our primary objective was to explore the utility of prospectively promising remote sensing data sources for mapping key forest attributes of the post-fire environment, including change relative to pre-fire conditions. In general, we find that DAP auxiliary information can facilitate these efforts when combined with Sentinel-2 pre- and post-fire images, which forms a low-cost alternative to lidar with complete spatial coverage of large areas. We note that our analysis relied on the availability of a lidar-derived digital terrain model for a region of interest, which is commonly available in western Oregon due to an extensive patchwork of previously collected lidar data. Analyses elsewhere lacking such lidar collections may need to rely on lower quality digital terrain models, such as those obtained from radar sensors, which may compromise model performance due to a lower coherence between heights obtained from the DAP point cloud and real tree heights (Strunk et al., 2019). In the context of our study, this would have the largest implications for models that rely heavily on canopy height predictors, like live aboveground biomass and live stem density (Fig. 4). DAP provided large gains in predictive performance for live aboveground biomass and relative basal area change relative to models fit using only multispectral imagery (Table 5), which is important to consider when contrasting our results with currently available multispectral derivatives (Ohmann and Gregory, 2002; Baker et al., 2020). However, our results indicate that DAP height predictors can deviate from lidar to a problematic degree when lidar canopy cover is less than 60 % (Fig. 9), due especially to the omission of standing dead trees with little or no retained live crown. DAP's incapacity to capture standing dead trees also compromised the performance of the standing dead aboveground biomass model. When forest managers are tasked with the quantification of standing dead aboveground biomass, e.g., when evaluating prospects for timber salvage, models based on DAP alone can be expected to produce large errors in regions of the fire where the salvage decision may be most germane.

While DAP and Sentinel-2 data provide an exciting opportunity to characterize post-fire conditions over entire states at low cost, the greatest explanatory power is achieved with lidar. Especially intriguing is our finding that post-fire lidar alone is sufficient to provide mapped predictions of four important post-fire forest monitoring attributes. In this region of the world, post-fire lidar acquisitions are not uncommon, with the Beachie Creek and Lionshead Fire acquisition, an acquisition encompassing the Douglas Complex (Galbraith et al., 2024; Lesmeister et al., 2019), and a forthcoming acquisition for the Riverside fire (a Labor Day 2020 fire located north of our study region) being examples of such an investment. Our results provide some justification for why explicit post-fire lidar data may be desirable. Lidar models for standing dead aboveground biomass, an attribute of outsized importance to inform forest management in post-fire settings, obtained much lower mean square errors than the corresponding DAP models (Table 6). This result appears to be driven by the more reliable quantification of the heights of dead trees and the availability of canopy intensity predictors (Fig. 4). We highlight that mean canopy intensity exhibited a negative trend in the accumulated local effects for relative basal area change, suggesting that burned components of tree canopies absorb more radiative energy than live components (Fig. 5). During our literature review of this topic, we found relatively little research that takes advantage of lidar intensity values in post-fire or fire effects analysis settings, with some notable exceptions (Hoe et al., 2018; Viedma et al., 2020; Galbraith et al., 2024), while the use of intensity predictors in other contexts, such as pre-fire fuel mapping, is more common (Erdody and Moskal, 2010; Filippelli et al., 2019; Stefanidou et al., 2020). This may be due to the recent development of new sensor technologies that allow the lidar sensor to actively normalize intensity values as they are collected in flight, rather than relying on intensity normalization methods conducted as a post-processing step (e.g., Gatziolis, 2011), which may have discouraged prior uptake. Given that lidar intensity predictors were important relative to other variables (Fig. 4), our results suggest that taking advantage of these new technologies is a high priority for post-fire forest monitoring and may provide justification for explicit post-fire lidar acquisitions in some cases.

Our study exists in a broader context of rapid DAP uptake for forest inventory mapping purposes, which has large implications for remote sensing of fire effects. Largely, the benefit of DAP is that of broad spatial coverage at frequent intervals (most recently, two-year time intervals in the United States) at low cost. Thus, it is likely that future mapping efforts will address larger and more ecologically diverse regions, such as entire states (e.g, Strunk et al., 2019; Schroeder et al., 2022). This study investigated the specific case of wildfires, a forest subpopulation that is of great importance to forest managers, and where DAP based predictive maps may well be relied upon to represent an array of attributes, including those assessed here. When combined with DAP, multispectral data from Sentinel-2 expanded the breadth of attributes that could be predicted with potentially acceptable accuracy by reducing some sources of error (Table 6), especially for standing dead aboveground biomass and relative basal area change.

### 5.3. Further research

Our results motivate further consideration of DAP information for post-fire mapping applications. Notably, we omitted any spectral information assigned to the DAP points when creating predictors for the post-fire random forest models. Although the available DAP data included spectral information for each point, an examination of potential DAP spectral predictors revealed topographic effects where slopes were steep, leading us to augment our models with Sentinel-2 Level 2A imagery instead. Spectral DAP information collected from these sensors could be improved by applying further topographic corrections and, if successfully calibrated, could then be used to obtain post-fire mapping relevant predictors such as vegetation indices that we calculated from the much coarser-scale Sentinel-2 (Prior et al., 2022). Further developments in DAP for post-fire monitoring might also address quantifying changes using pre- and post-fire DAP acquisitions, which will become more common as DAP is continually collected over the same regions. Benefits form this line of research are analogous to those suggested by studies that address wildfire effects using bi-temporal lidar acquisitions (Hoe et al., 2018; McCarley et al., 2020).

Our approach in this study required the availability of field data obtained directly from a post-fire region of interest. Furthermore, we used a unique field data set that contains post-fire remeasurements on field plots within burn perimeters very soon after fire. Existing institutional wildfire mapping efforts such as MTBS and RAVG, which may not rely explicitly on a post-fire sample obtained for a specific fire (Baker et al., 2020), achieve rapid delivery of mapping products to forest managers. Our results are likely optimistic compared to normal post-fire sampling intensities, which are typically much smaller in the western United States (Affleck and Gaines, 2023). However, as broad-scale remote sensing information sources like DAP, Sentinel-2 and others are continually collected in parallel with national forest inventory information, an opportunity exists to create models that use field data that are temporally or spatially external to any given fire of interest while yielding predictions of post-fire forest attributes. Recent efforts in small area estimation can be applied to facilitate this type of analysis (Gaines and Affleck, 2021; Wiener et al., 2021), and further research is warranted to investigate these techniques and how they can support rapid delivery of post-fire forest maps that rely on DAP or other remote sensing data while incorporating field information from national forest inventory plots.

## 6. Conclusion

In this study, we compared regression models using digital aerial photogrammetric point clouds (DAP) and lidar point clouds in a post-fire forest mapping context. Lidar models attained the best prediction performance across all attributes we examined, driven primarily by higher quality height and cover predictors and the availability of lidar intensity. While lidar-driven models overall attained the best prediction performance, we found that augmenting DAP data with pre- and post-fire Sentinel-2 imagery reduced the discrepancy in prediction performance between lidar and DAP-driven models. The discrepancy between live aboveground biomass and live stem density was relatively small after the inclusion of Sentinel-2 data, while discrepancies between standing dead aboveground biomass and relative basal area change were larger. An examination of height predictors from lidar and DAP revealed large discrepancies, which was found to occur primarily when lidar cover was below 60 % and with low lidar canopy intensity values, suggesting that consumption of canopy fuels leads to errors in DAP height predictors. DAP data is broadly available at low cost, making it attractive for producing routine large-scale inventory maps. Inclusion of Sentinel-2 or other multispectral information will be important when generating map products for which post-fire environments are a subpopulation of interest to end users.

## CRediT authorship contribution statement

**Bryce Frank**: Writing – original draft, Visualization, Validation, Methodology, Investigation, Formal analysis, Data curation, Conceptualization. **Jacob L. Strunk**: Writing – review & editing, Methodology, Investigation, Data curation, Conceptualization. **Jeremy S. Fried**: Writing – review & editing, Data curation, Conceptualization. **Karin Wolken:** Writing – review & editing, Conceptualization. **Sean C. McKenzie**: Writing – review & editing, Data curation, Conceptualization.

## Declaration of Competing Interest

The authors declare that they have no known competing financial interests or personal relationships that could have appeared to influence the work reported in this paper.

## Acknowledgements

We gratefully acknowledge the team of forest managers at USDA Forest Service Region 6, USDA Forest Service Pacific Northwest Research Station, Washington Department of Natural Resources, Oregon Department of Forestry, and the Bureau of Land Management that provided initial input for our analysis. This material is based upon work supported by the United States Geological Survey under Grant/Cooperative Agreement No. G22AC00258-00.

## Appendix A. Supporting information

Supplementary data associated with this article can be found in the online version at doi:10.1016/j.foreco.2025.123002.

## Data availability

The data that has been used is confidential.

## References

Affleck, D.L.R., Gaines, G.C., 2023. Model-assisted domain estimation of postfire tree regeneration in the western US using nearest neighbor techniques. Can. J. For. Res. 53, 981–995. https://doi.org/10.1139/cjfr-2023-0007.

Ali-Sisto, D., Packalen, P., 2016. Forest change detection by using point clouds from dense image matching together with a LiDAR-derived terrain model. IEEE J. Sel. Top. Appl. Earth Obs. Remote Sens. 10, 1197–1206.

Andersen, H.-E., Reutebuch, S.E., McGaughey, R.J., 2006. A rigorous assessment of tree height measurements obtained using airborne lidar and conventional field methods. Can. J. Remote Sens. 32, 355–366. https://doi.org/10.5589/m06-030.

Apley, D.W., Zhu, J., 2020. Visualizing the effects of predictor variables in black box supervised learning models. J. R. Stat. Soc. Ser. B Stat. Method. 82, 1059–1086. https://doi.org/10.1111/rssb.12377.

Baker, C., Harvey, B., Saberi, S., Reiner, A., Wahlberg, M., 2020. Regionally adapted models for the rapid assessment of vegetation condition after wildfire program in the interior Northwest and Southwest United States. For. Manag. Partnersh. 6.

Bates, S., Hastie, T., Tibshirani, R., 2024. Cross-validation: what does it estimate and how well does it do it? J. Am. Stat. Assoc. 119, 1434–1445. https://doi.org/10.1080/01621459.2023.2197686.

Bechtold, W.A., Scott, C.T., 2005. The forest inventory and analysis plot design. Enhanced Forest Inventory Analysis Program–National Sampling Design and Estimation Procedures, pp. 27–42.
Beck, H.E., McVicar, T.R., Vergopolan, N., Berg, A., Lutsko, N.J., Dufour, A., Zeng, Z., Jiang, X., van Dijk, A.I., Miralles, D.G., 2023. High-resolution (1 km) Köppen-Geiger maps for 1901–2099 based on constrained CMIP6 projections. Sci. Data 10, 724.
Bohlin, I., Olsson, H., Bohlin, J., Granström, A., 2017. Quantifying post-fire fallen trees using multi-temporal lidar. Int. J. Appl. Earth Obs. Geoinf. 63, 186–195. https://doi.org/10.1016/j.jag.2017.08.004.
Breidenbach, J., Magnussen, S., Rahlf, J., Astrup, R., 2018. Unit-level and area-level small area estimation under heteroscedasticity using digital aerial photogrammetry data. Remote Sens. Environ. 212, 199–211. https://doi.org/10.1016/j.rse.2018.04.028.
Bright, B.C., Hudak, A.T., McGaughey, R., Andersen, H.-E., Negrón, J., 2013. Predicting live and dead tree basal area of bark beetle affected forests from discrete-return lidar. Can. J. Remote Sens. 39, S99–S111. https://doi.org/10.5589/m13-027.
Busby, S.U., Klock, A.M., Fried, J.S., 2023. Inventory analysis of fire effects wrought by wind-driven megafires in relation to weather and pre-fire forest structure in the western Cascades. Fire Ecol. 19, 58. https://doi.org/10.1186/s42408-023-00219-x.
Chamberlain, C.P., Meador, A.J.S., Thode, A.E., 2021. Airborne lidar provides reliable estimates of canopy base height and canopy bulk density in southwestern ponderosa pine forests. For. Ecol. Manag. 481, 118695. https://doi.org/10.1016/j.foreco.2020.118695.
Chuvieco, E., Martín, M.P., Palacios, A., 2002. Assessment of different spectral indices in the red-near-infrared spectral domain for burned land discrimination. Int. J. Remote Sens. 23, 5103–5110. https://doi.org/10.1080/01431160210153129.
Clark, J., Parsons, A., Zajkowski, T., Lannom, K., 2003. Remote Sensing Imagery Support for Burned Area Emergency Response Teams on 2003 Southern California Wildfires. USFS Remote Sensing Application Center BAER Support Summary.
Core Team, R., 2024. R: A Language and Environment for Statistical Computing. R Foundation for Statistical Computing, Vienna, Austria.
Dietmaier, A., McDermid, G.J., Rahman, M.M., Linke, J., Ludwig, R., 2019. Comparison of LiDAR and digital aerial photogrammetry for characterizing canopy openings in the Boreal Forest of Northern Alberta. Remote Sens. 11, 1919. https://doi.org/10.3390/rs11161919.
Eidenshink, J., Schwind, B., Brewer, K., Zhu, Z.-L., Quayle, B., Howard, S., 2007. A project for monitoring trends in burn severity. Fire Ecol. 3, 3–21. https://doi.org/10.4996/fireecology.0301003.
Erdody, T.L., Moskal, L.M., 2010. Fusion of LiDAR and imagery for estimating forest canopy fuels. Remote Sens. Environ. 114, 725–737.
Fassnacht, F.E., White, J.C., Wulder, M.A., Næsset, E., 2024. Remote sensing in forestry: current challenges, considerations and directions. For. Int. J. For. Res. 97, 11–37. https://doi.org/10.1093/forestry/cpad024.
Filippelli, S.K., Lefsky, M.A., Rocca, M.E., 2019. Comparison and integration of lidar and photogrammetric point clouds for mapping pre-fire forest structure. Remote Sens. Environ. 224, 154–166.
Gaines III, G.C., Affleck, D.L., 2021. Small area estimation of postfire tree density using continuous forest inventory data. Front. For. Glob. Change 4, 761509.
Galbraith, S.M., Valente, J.J., Dunn, C.J., Rivers, J.W., 2024. Both Landsat- and LiDAR-derived measures predict forest bee response to large-scale wildfire. Remote Sens. Ecol. Conserv. 10, 24–38. https://doi.org/10.1002/rse2.354.
Gatziolis, D., 2011. Dynamic range-based intensity normalization for airborne, discrete return lidar data of forest canopies. Photogramm. Eng. Remote Sens. 77, 251–259. https://doi.org/10.14358/pers.77.3.251.
Goodbody, T.R., Coops, N.C., Hermosilla, T., Tompalski, P., McCartney, G., MacLean, D. A., 2018. Digital aerial photogrammetry for assessing cumulative spruce budworm defoliation and enhancing forest inventories at a landscape-level. ISPRS J. Photogramm. Remote Sens. 142, 1–11.
Hoe, M.S., Dunn, C.J., Temesgen, H., 2018. Multitemporal LiDAR improves estimates of fire severity in forested landscapes. Int. J. Wildland Fire 27, 581–594. https://doi.org/10.1071/wf17141.
Honkavaara, E., Litkey, P., Nurminen, K., 2013. Automatic storm damage detection in forests using high-altitude photogrammetric imagery. Remote Sens. 5, 1405–1424.
Hooker, G., Mentch, L., Zhou, S., 2021. Unrestricted permutation forces extrapolation: variable importance requires at least one more model, or there is no free variable importance. Stat. Comput. 31, 82. https://doi.org/10.1007/s11222-021-10057-z.
Hu, T., Ma, Q., Su, Y., Battles, J.J., Collins, B.M., Stephens, S.L., Kelly, M., Guo, Q., 2019. A simple and integrated approach for fire severity assessment using bi-temporal airborne LiDAR data. Int. J. Appl. Earth Obs. Geoinf. 78, 25–38. https://doi.org/10.1016/j.jag.2019.01.007.
Key, C.H., Benson, N.C., 2005. Landscape assessment: remote sensing of severity, the normalized burn ratio and ground measure of severity, the composite burn index. FIREMON: Fire Effects Monitoring and Inventory System. USDA Forest Service, Rocky Mountain Research Station, Ogden, UT, p. 108.
Larson, A.J., Jeronimo, S.M., Hessburg, P.F., Lutz, J.A., Povak, N.A., Cansler, C.A., Kane, V.R., Churchill, D.J., 2022. Tamm review: ecological principles to guide post-fire forest landscape management in the Inland Pacific and Northern Rocky Mountain regions. For. Ecol. Manag. 504, 119680. https://doi.org/10.1016/j.foreco.2021.119680.
Lentile, L.B., Holden, Z.A., Smith, A.M., Falkowski, M.J., Hudak, A.T., Morgan, P., Lewis, S.A., Gessler, P.E., Benson, N.C., 2006. Remote sensing techniques to assess active fire characteristics and post-fire effects. Int. J. Wildland Fire 15, 319–345. https://doi.org/10.1071/wf05097.
Lesmeister, D.B., Sovern, S.G., Davis, R.J., Bell, D.M., Gregory, M.J., Vogeler, J.C., 2019. Mixed-severity wildfire and habitat of an old-forest obligate. Ecosphere 10, e02696. https://doi.org/10.1002/ecs2.2696.
Li, K., Xu, E., 2023. Differentiating effects of salvage logging and recovery patterns on post-fire boreal forests in Northeast China using a modified forest disturbance index. GIScience Remote Sens. 60, 2188674. https://doi.org/10.1080/15481603.2023.2188674.
Lindenmayer, D.B., Foster, D.R., Franklin, J.F., Hunter, M.L., Noss, R.F., Schmiegelow, F. A., Perry, D., 2004. Salvage harvesting policies after natural disturbance. Science 303, 1303. https://doi.org/10.1126/science.1093438.
Mauro, F., Hudak, A.T., Fekety, P.A., Frank, B., Temesgen, H., Bell, D.M., Gregory, M.J., McCarley, T.R., 2021. Regional modeling of forest fuels and structural attributes using airborne laser scanning data in Oregon. Remote Sens. 13, 261. https://doi.org/10.3390/rs13020261.
McCarley, T.R., Hudak, A.T., Sparks, A.M., Vaillant, N.M., Meddens, A.J.H., Trader, L., Mauro, F., Kreitler, J., Boschetti, L., 2020. Estimating wildfire fuel consumption with multitemporal airborne laser scanning data and demonstrating linkage with MODIS-derived fire radiative energy. Remote Sens. Environ. 251, 112114. https://doi.org/10.1016/j.rse.2020.112114.
Meng, R., Wu, J., Schwager, K.L., Zhao, F., Dennison, P.E., Cook, B.D., Brewster, K., Green, T.M., Serbin, S.P., 2017. Using high spatial resolution satellite imagery to map forest burn severity across spatial scales in a Pine Barrens ecosystem. Remote Sens. Environ. 191, 95–109. https://doi.org/10.1016/j.rse.2017.01.016.
Mielcarek, M., Kamińska, A., Stereńczak, K., 2020. Digital aerial photogrammetry (DAP) and airborne laser scanning (ALS) as sources of information about tree height: comparisons of the accuracy of remote sensing methods for tree height estimation. Remote Sens. 12, 1808.
Miller, J.D., Knapp, E.E., Key, C.H., Skinner, C.N., Isbell, C.J., Creasy, R.M., Sherlock, J. W., 2009. Calibration and validation of the relative differenced normalized burn ratio (RdNBR) to three measures of fire severity in the Sierra Nevada and Klamath Mountains, California, USA. Remote Sens. Environ. 113, 645–656. https://doi.org/10.1016/j.rse.2008.11.009.
Molnar, C., Casalicchio, G., Bischl, B., 2018. Iml: an R package for interpretable machine learning. J. Open Source Softw. 3, 786. https://doi.org/10.21105/joss.00786.
Moradi, F., Darvishsefat, A.A., Pourrahmati, M.R., Deljouei, A., Borz, S.A., 2022. Estimating aboveground biomass in dense Hyrcanian forests by the use of Sentinel-2 data. Forests 13, 104. https://doi.org/10.3390/f13010104.
Ohmann, J.L., Gregory, M.J., 2002. Predictive mapping of forest composition and structure with direct gradient analysis and nearest- neighbor imputation in coastal Oregon, U.S.A. Can. J. For. Res. 32, 725–741. https://doi.org/10.1139/x02-011.
Picotte, J.J., Bhattarai, K., Howard, D., Lecker, J., Epting, J., Quayle, B., Benson, N., Nelson, K., 2020. Changes to the monitoring trends in burn severity program mapping production procedures and data products. Fire Ecol. 16, 16. https://doi.org/10.1186/s42408-020-00076-y.
Prior, E.M., Thomas, V.A., Wynne, R.H., 2022. Estimation of mean dominant height using NAIP digital aerial photogrammetry and lidar over mixed deciduous forest in the southeastern USA. Int. J. Appl. Earth Obs. Geoinf. 110, 102813.
Qi, J., Chehbouni, A., Huete, A.R., Kerr, Y.H., Sorooshian, S., 1994. A modified soil adjusted vegetation index. Remote Sens. Environ. 48, 119–126. https://doi.org/10.1016/0034-4257(94)90134-1.
Reams, G.A., Smith, W.D., Hansen, M.H., Bechtold, W.A., Roesch, F.A., Moisen, G.G., 2005. The forest inventory and analysis sampling frame. The Enhanced Forest Inventory and Analysis Program—National Sampling Design and Estimation Procedures, p. 11.
Ritz, A.L., Thomas, V.A., Wynne, R.H., Corey Green, P., Schroeder, T.A., Albaugh, T.J., Burkhart, H.E., Carter, D.R., Cook, R.L., Campoe, O.C., Rubilar, R.A., Rakestraw, J., 2022. Assessing the utility of NAIP digital aerial photogrammetric point clouds for estimating canopy height of managed loblolly pine plantations in the southeastern United States. Int. J. Appl. Earth Obs. Geoinf. 113, 103012. https://doi.org/10.1016/j.jag.2022.103012.
Rodman, K.C., Fornwalt, P.J., Holden, Z.A., Crouse, J.E., Davis, K.T., Marshall, L.A.E., Stoddard, M.T., Andrus, R.A., Chambers, M.E., Chapman, T.B., Hart, S.J., Schloegel, C.A., Stevens-Rumann, C.S., 2024. Green is the New Black: outcomes of post-fire tree planting across the US Interior West. For. Ecol. Manag. 574, 122358. https://doi.org/10.1016/j.foreco.2024.122358.
Roussel, J.-R., Auty, D., Coops, N.C., Tompalski, P., Goodbody, T.R., Meador, A.S., Bourdon, J.-F., De Boissieu, F., Achim, A., 2020. lidR: an R package for analysis of Airborne Laser Scanning (ALS) data. Remote Sens. Environ. 251, 112061. https://doi.org/10.1016/j.rse.2020.112061.
Schroeder, T.A., Obata, S., Papeş, M., Branoff, B., 2022. Evaluating statewide NAIP photogrammetric point clouds for operational improvement of national forest inventory estimates in mixed hardwood forests of the Southeastern US. Remote Sens. 14, 4386. https://doi.org/10.3390/rs14174386.
Sheridan, R., Popescu, S., Gatziolis, D., Morgan, C., Ku, N.-W., 2015. Modeling forest aboveground biomass and volume using airborne LiDAR metrics and forest inventory and analysis data in the Pacific Northwest. Remote Sens. 7, 229–255. https://doi.org/10.3390/rs7010229.
Shi, T., Xu, H., 2019. Derivation of tasseled cap transformation coefficients for Sentinel-2 MSI At-sensor reflectance data. IEEE J. Sel. Top. Appl. Earth Obs. Remote Sens. 12, 4038–4048. https://doi.org/10.1109/jstars.2019.2938388.
Shin, J., Temesgen, H., Strunk, J.L., Hilker, T., 2016. Comparing modeling methods for predicting forest attributes using LiDAR metrics and ground measurements. Can. J. Remote Sens 42, 739–765. https://doi.org/10.1080/07038992.2016.1252908.
Stefanidou, A., Z. Gitas, I., Korhonen, L., Georgopoulos, N., Stavrakoudis, D., 2020. Multispectral lidar-based estimation of surface fuel load in a dense coniferous forest. Remote Sens. 12, 3333.
Strunk, J., Packalen, P., Gould, P., Gatziolis, D., Maki, C., Andersen, H.-E., McGaughey, R.J., 2019. Large area forest yield estimation with pushbroom digital aerial photogrammetry. Forests 10, 397. https://doi.org/10.3390/f10050397.

Strunk, J., Cosenza, D.N., Mauro, F., Andersen, H.-E., de Bruin, S., Bryant, T., Packalen, P., 2025. Mitigation of spatial effects on an area-based lidar forest inventory (2024). IEEE J. Sel. Top. Appl. Earth Obs. Remote Sens.

Strunk, J.L., Gould, P.J., Packalen, P., Gatziolis, D., Greblowska, D., Maki, C., McGaughey, R.J., 2020. Evaluation of pushbroom DAP relative to frame camera DAP and lidar for forest modeling. Remote Sens. Environ. 237, 111535.

Temesgen, H., Mauro, F., Hudak, A.T., Frank, B., Monleon, V., Fekety, P., Palmer, M., Bryant, T., 2021. Using Fay–Herriot models and variable radius plot data to develop a stand-level inventory and update a prior inventory in the Western Cascades, OR, United States. Front. For. Glob. Change 4, 745916. https://doi.org/10.3389/ffgc.2021.745916.

Tian, L., Wu, X., Tao, Y., Li, M., Qian, C., Liao, L., Fu, W., 2023. Review of remote sensing-based methods for forest aboveground biomass estimation: progress, challenges, and prospects. Forests 14, 1086. https://doi.org/10.3390/f14061086.

Tucker, C.J., 1979. Red and photographic infrared linear combinations for monitoring vegetation. Remote Sens. Environ. 8, 127–150. https://doi.org/10.1016/0034-4257(79)90013-0.

USDA Forest Service, 2023. Field Instructions for the Annual Inventory of California, Oregon, and Washington.

Viedma, O., Almeida, D.R., Moreno, J.M., 2020. Postfire tree structure from high-resolution LiDAR and RBR sentinel 2A fire severity metrics in a Pinus halepensis-dominated burned stand. Remote Sens. 12, 3554. https://doi.org/10.3390/rs12213554.

Vogeler, J.C., Yang, Z., Cohen, W.B., 2016. Mapping post-fire habitat characteristics through the fusion of remote sensing tools. Remote Sens. Environ. 173, 294–303. https://doi.org/10.1016/j.rse.2015.08.011.

Westfall, J.A., Coulston, J.W., Gray, A.N., Shaw, J.D., Radtke, P.J., Walker, D.M., Weiskittel, A.R., MacFarlane, D.W., Affleck, D.L., Zhao, D., 2024. A National-scale Tree Volume, Biomass, and Carbon Modeling System for the United States. General Technical Report WO-104. US Department Agriculture, Forest Service, Washington, DC, p. 104.

Wiener, S.S., Bush, R., Nathanson, A., Pelz, K., Palmer, M., Alexander, M.L., Anderson, D., Treasure, E., Baggs, J., Sheffield, R., 2021. United States forest service use of forest inventory data: examples and needs for small area estimation. Front. For. Glob. Change 4, 763487. https://doi.org/10.3389/ffgc.2021.763487.

Winsemius, S., Babcock, C., Kane, V.R., Bormann, K.J., Safford, H.D., Jin, Y., 2024. Improved aboveground biomass estimation and regional assessment with aerial lidar in California's subalpine forests. Carbon Balance Manag. 19, 41. https://doi.org/10.1186/s13021-024-00286-w.

Woebbecke, D.M., Meyer, G.E., Von Bargen, K., Mortensen, D.A., 1995. Color indices for weed identification under various soil, residue, and lighting conditions. Trans. ASAE 38, 259–269. https://doi.org/10.13031/2013.27838.

Wright, M.N., Ziegler, A., 2017. Ranger: a fast implementation of random forests for high dimensional data in C++ and R. J. Stat. Softw. 77. https://doi.org/10.18637/jss.v077.i01.

Zhou, Y., Feng, Z., 2023. Estimation of forest stock volume using Sentinel-2 MSI, Landsat 8 OLI imagery and forest inventory data. Forests 14, 1345. https://doi.org/10.3390/f14071345.